8-31-2023

Investigating the rheological behavior of a simple yield stress fluid under shear flows

Francesco Accetta
New Jersey Institute of Technology, francesco.accetta18@gmail.com

ABSTRACT

INVESTIGATING THE RHEOLOGICAL BEHAVIOR OF A SIMPLE YIELD STRESS FLUID UNDER SHEAR FLOWS

by
Francesco Accetta

Many soft materials display unique and complex rheological behavior characterized by a transition from a solid-like to a fluid-like state upon the application of a force that exceeds the threshold to flow, known as the yield stress. Yield stress fluids are found in a wide range of commonly encountered materials including microgels, emulsions, and foams, and have been widely studied by rheologists over the last several decades. Carbopol is a popular polymeric microgel system as it displays simple, non-thixotropic rheological behavior and is typically seen as an ideal yield stress fluid. Previous research has demonstrated the reproducible behavior of shear stress in Carbopol systems, but measurements of the normal stress differences are either limited in scope or demonstrate chaotic behavior. Here a Carbopol yield stress fluid is evaluated to examine how experimental test history effects subsequent constant shear strain rate experiments, and how the shear stress and normal stress differences evolve during and after being subject to a period of zero stress known as recovery.

INVESTIGATING THE RHEOLOGICAL BEHAVIOR OF A SIMPLE YIELD STRESS FLUID UNDER SHEAR FLOWS

by
Francesco Accetta

A Thesis
Submitted to the Faculty of
New Jersey Institute of Technology
in Partial Fulfillment of the Requirements for the Degree of
Master of Materials Engineering

Otto H. York Department of
Chemical and Materials Engineering

August 2023

APPROVAL PAGE

**INVESTIGATING RHEOLOGICAL BEHAVIOR OF CARBOPOL
YIELD STRESS FLUID**

Francesco Accetta

Dr. David Venerus, Thesis Advisor	Date
Professor of Chemical and Materials Engineering, NJIT	

Dr. Kathleen McEnnis, Committee Member	Date
Assistant Professor of Chemical and Materials Engineering, NJIT	

Dr. Murat Guvendiren, Committee Member	Date
Associate Professor of Chemical and Materials Engineering, NJIT	

BIOGRAPHICAL SKETCH

Author: Francesco Accetta

Degree: Master of Science

Date: August 2023

Date of Birth:

Place of Birth:

Undergraduate and Graduate Education:

- Master of Science
  New Jersey Institute of Technology, Newark, NJ 2023

- Bachelor of Science in Engineering Chemistry and Chemistry
  Stony Brook University, Stony Brook, NY, 2018

Major: Materials Engineering

To my boys, Casper and Tanner, for years of laughter and unconditional love, and many late nights of studying and snacks.

ACKOWLEDGEMENT

TABLE OF CONTENTS

LIST OF TABLES

LIST OF FIGURES

CHAPTER 1

INTRODUCTION

1.1 Objective

The objective of this study is to investigate the behavior of normal stresses in a Carbopol rheological system under shear flows. Various test geometries and parameters were employed to examine the rheological behavior of Carbopol and enhance our understanding of the influence of test protocols on the nature of the normal stress responses.

Multiple rheometers, employing both cone-plate (CP) and parallel-plate (PP) geometries, were used to measure the yield stress, shear stress, and normal stress differences. The key experiments involved constant strain rate tests, with waiting periods defined by two distinct conditions: either constant strain relaxation or constant stress recovery. These protocols aim to reveal the impact of test history on the stress response of yield stress fluids.

1.2 Shear Rheology

Rheology, the study of the flow and deformation of soft matter, explores the relationship between stress, deformation, and time. While it encompasses the deformation of solid-like materials, its primary focus lies in understanding the flow behavior of liquid-like and complex viscoelastic materials, which exhibit characteristics of both solids and liquids [5]. In fluid rheology studies, shear flow is commonly considered, which involves the movement of fluid layers past one another with a velocity gradient between the applied

force on the moving top layer and the stationary bottom layer. In practice, a fluid sample is typically placed between two plates separated by a gap (*H*). These plates consist of a stationary bottom plate and a moving top plate, which is subjected to a known force (*F*) acting on a specific sample area (*A*) and moves at a known velocity (*V*). The resulting ratio is expressed as the shear stress (σ), given by the equation

$$\sigma = \frac{F}{A} \tag{1.1}$$

with units of [N/m²] or [Pa]. Due to the difference in velocity of adjacent layers in the fluid, a velocity gradient develops in the sample that is represented by the shear rate ($\dot{\gamma}$), a measure of the change in strain with time

$$\dot{\gamma} = \frac{\partial v_1}{dx_2} = \frac{V}{H} \tag{1.2}$$

with units of [s⁻¹] and is the slope of the velocity gradient that develops during shear flow (Figure 1.1.)
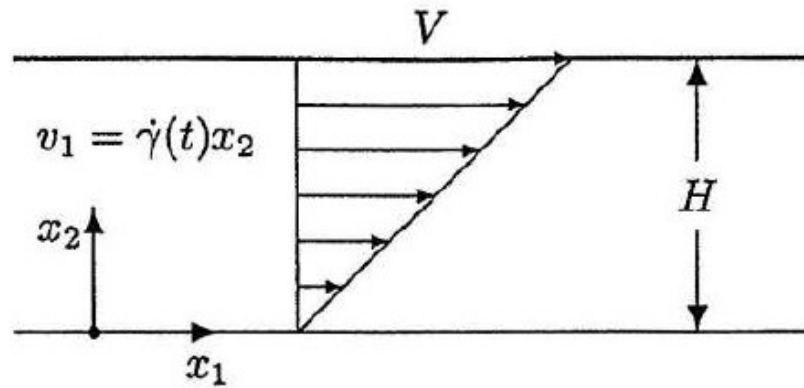
Figure 1.1 Time dependent shear flow between parallel plates with shear rate $\dot{\gamma}(t)$. [6]

The ratio of the shear stress and shear strain rate is determined by the viscosity η, where

$$\eta = \frac{\sigma}{\dot{\gamma}}$$

(1.3)

with units of Pascal seconds [Pa·s]. Fluids that have a linear relationship between shear stress and strain, or a constant viscosity independent of the shear rate, are referred to as Newtonian fluids. Fluids that have a viscosity that depends on the shear rate are broadly termed non-Newtonian and can be classified further into other categories based on their rheological behavior, which can be seen in Figure 1.2. Each of the categories has multiple models that can be used to represent their behavior but are not necessary for the work presented here. If the upper surface is displaced by a distance L, the shear strain (γ) is

$$\gamma = \frac{L}{H}$$

(1.4)

and the ratio of the shear stress to the shear strain is the shear modulus G,

$$G = \frac{\sigma}{\gamma}.$$

(1.5)

One of the most common rheological measurements is oscillatory shear, often categorized as small- or large-amplitude oscillatory shear (SAOS or LAOS) . For this work, the test conducted is known as the oscillatory frequency sweep test.
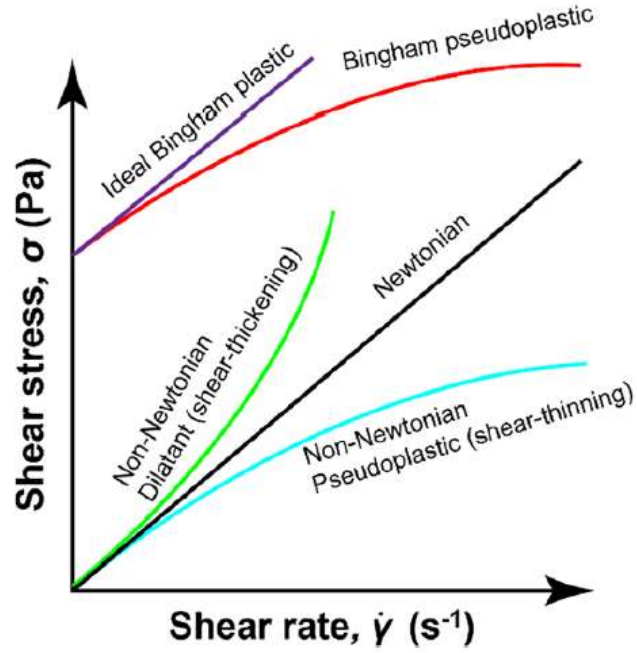
Figure 1.2 Shear stress versus shear rate various fluid classifications.

Source: [1]

These tests give information on the time dependent stress response of the material by applying a sinusoidal strain with an angular frequency ω, as

$$\gamma(t) = \gamma_0 sin(\omega t) \tag{1.6}$$

where γ_0 << 1 for SAOS, allowing for the viscoelastic response to be measured on different time scales [5, 7]. The sinusoidal strain is applied to the sample and the stress response is measured as

$$\sigma(t) = \sigma_0 \sin(\omega t + \delta) \tag{1.7}$$

where δ is known as the phase angle [7, 8]. The phase angle represents the lag between the shear stress from the applied strain. For perfectly elastic materials $\delta = 0°$; for purely Newtonian fluids $\delta = 90°$; and in viscoelastic materials δ will fall between 0 and 90°, with 45° representing the boundary between solid-like and liquid-like behavior [5]. Because the stress response is also sinusoidal with the same frequency as the applied strain, a complex modulus G^* can be developed, with

$$G^* = \frac{\tau_0}{\gamma_0} = G' sin\omega + iG'' cos\omega \tag{1.8}$$

where τ_0/γ_0 is the shear modulus amplitude at a given frequency, and G' and G'' are storage and loss moduli, respectively, that are related to the materials storage and dissipation of energy during deformation, which are given by

$$G'(\omega) = \frac{\tau_0}{\gamma_0} cos\delta \tag{1.9}$$

$$G''(\omega) = \frac{\tau_0}{\gamma_0} sin\delta. \tag{1.10}$$

In viscoelastic systems, the phase angle is typically expressed as the loss tangent (tan δ) and represents the ratio between G' and G'' as

$$tan\,(\delta) = \frac{G''}{G'}. \tag{1.11}$$

This culminates in producing diagrams (Figure 1.3) that give insight regarding the viscoelastic behavior of the fluid by creating plots of G' and G'' against the angular frequency, where various classes of fluids exhibit characteristic behavior of the storage and loss moduli. Because experiments are run on multiple samples throughout this work, frequency sweeps will verify that each sample evaluated has the same microstructural arrangement so rheological measurements are reliable.
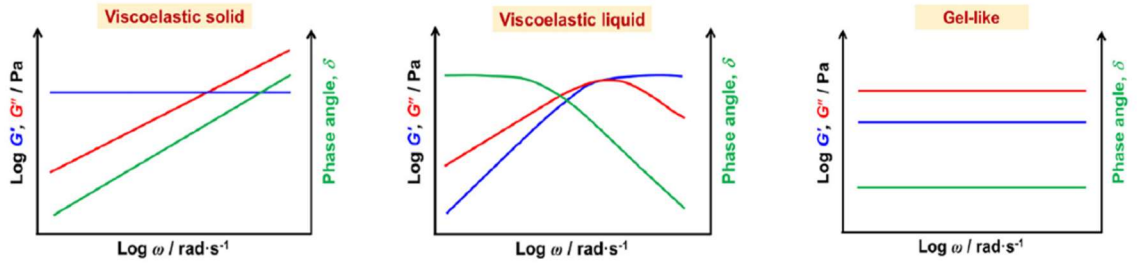
Figure 1.3 Typical G', G'', and δ for viscoelastic solid, viscoelastic liquid, and gel-like materials.

Source: [1]

A low frequency approximation can be sued to determine the shear modulus G from G', since at low frequencies the response of a viscoelastic solid is strongly dominated by the storage modulus, meaning that $G' >> G''$ [7]. The low frequency limit is given as,

$$G = \lim_{\omega \to 0} G'(\omega). \tag{1.12}$$

and will be used in later analysis to determine the shear modulus for the sample tested.

1.3 Yield Stress Fluids

Yield stress fluids have become a prominent area of interest in rheological research due to their unique and complex behavioral phenomena. These fluids comprise materials such as microgels, emulsions, and foams, and are commonly found in everyday household products like hair gels, lotions, and food items, as well as in various industrial applications including crude oil, mortars, and cement. What sets yield stress fluids apart is their characteristic behavior: they exhibit solid-like elastic properties until they are subjected to a force that surpasses their threshold to flow, known as the yield stress. Beyond this threshold, they exhibit the behavior of a viscous liquid. This physical phenomenon is often referred to as elastoviscoplastic behavior.

One of the biggest questions that remains open in the field of rheology is what exactly defines the yield stress. While the mechanics of Newtonian fluid flow have been extensively studied and modeled, fluids such as microgels, foams and emulsions demonstrate complex flow characteristics. These fluid categories are collectively known as yield stress fluids, as they display properties that encompass both solid-like and fluid-like behavior. However, the underlying physical phenomena that govern this yielding behavior is difficult to describe [2, 9].

A classic example of an everyday yield stress fluid frequently discussed in literature is whipped cream. When placed on a surface, whipped cream retains its shape, acting as a solid. The structure of whipped cream traps air bubbles, preventing their escape when undisturbed. However, when a utensil is passed through the whipped cream, it readily spreads, resembling the behavior of a viscous liquid. This is commonly juxtaposed with syrup or honey, both highly viscous liquids that readily flow and therefore do not show any signs of solid-like behavior, indicating that no solid structure

develops like the whipped cream. The yield stress serves as a crucial physical parameter that aids in comprehending the solid-to-liquid transition in whipped cream. However, among rheologists, there exists some debate regarding the precise definition and interpretation of the yield stress, giving rise to two primary viewpoints. The first perspective suggests that the yield stress denotes the transition between a solid and liquid state. Conversely, the second viewpoint posits that the yield stress solely represents the transition between two fluid states characterized by significantly different viscosities. Resolving this conflict extends beyond the scope of this study, but it underscores the presence of numerous unanswered questions in yield stress rheology. For the purposes of this study, the yield stress will be considered to align with the former argument, representing the transition from a solid to a liquid state.

Describing the solid-to-liquid transition in yield stress fluids poses a considerable challenge. Traditionally, when researchers discuss the yielding behavior of a solid material, there exists an initial structure that governs its mechanical properties, and once yielding takes place, the material undergoes irreversible changes known as plastic deformation. The behavior of these materials can be effectively explained by considering the movements of structural defects, including dislocations, impurities, or grain boundaries within the material's structure. In contrast, yield stress fluids have the unique ability to revert to a solid-like state once the yielding and flow have ceased, suggesting a process of rebuilding the initial microstructure when the applied force is removed. This indicates that the deformation behavior of yield stress fluids lacks the simple deformation mechanisms seen in solids. The microstructural origins of this flow behavior have been extensively investigated by numerous research groups using a combination of physical

experimentation and computer modeling across a range of fluid systems [3, 10-16]. It is difficult to develop constitutive equations that encompass all aspects of deformation for these materials as microstructure can vary widely from one material to the next. Microgels behavior is dictated by the polymer concentration and the degree of crosslinking that impacts how stresses are distributed through the network. Polymer chains stretch and deform without moving past one another until sufficient force is applied, breaking chains, and allowing small aggregates to flow past one another. Foams, emulsions, and suspensions consist of colloidal spheres that are considered to flow past one another under an applied force, whose behavior depends on adhesive or repulsive effects [16, 17], interfacial phenomenon[18, 19] or others depending on the material [16, 20].

Various rheological tests can be employed to measure the properties of yield stress fluids, and a subset of these tests will be utilized in this study. One commonly used rheological test is the shear rate ramp test. In this test, shear rates are gradually increased and then decreased in a series of steady-state steps to construct a flow curve. It is crucial to carefully control the shear rate steps in this experiment since there is evidence suggesting that the yield stress of the fluid may exhibit variation based on its flow history [21]. Ensuring sufficient time for the material to reach a steady state at each shear rate is crucial because there are slight differences between measurements of the yield stress when shear rates are increased versus decreased. When the shear rate is increased, the fluid undergoes a transition from a solid-like state to a fluid-like state, yielding the measurement of the static yield stress. Conversely, when the shear rate is decreased, the fluid undergoes a transition from a liquid-like state to a solid-like state, resulting in the

measurement of the dynamic yield stress. This suggests that the flow behavior of the material may be dependent on the conditions of the flow itself. When a yield stress fluid exhibits such behavior, it is said to be thixotropic.

The thixotropic response is related to the time dependent microstructural rearrangements that occur during deformation that can be partially destroyed during shear flow [2, 5]. A thixotropic yield stress fluid will have a viscosity and yield stress that decreases under any flow that liquefies the material [22], but will returns to its original value given sufficient time. The fluid response will depend on the rate at which the shear rate is ramped, and the rest time between measurements [2]. In contrast, a nonthixotropic fluid will maintain its viscosity and yield stress without any time dependence, whose stress response depends only on the shear rate [23]. Figure 1.4 shows the difference between a nonthixotropic Carbopol and thixotropic bentonite solution [2, 3]. Nonthixotropic materials develop a flow curve with no hysteresis (Fig. 1.4a), while thixotropic materials develop a large hysteresis loop during shear rate ramp tests (Fig. 1.4b). After ensuring the accuracy of the flow curve, the data can be fitted using a suitable model to determine the yield stress. In this study, like many others, the Herschel-Bulkley model (1.17) will be employed to fit the data. The flow curve obtained by decreasing shear rates will be used for extrapolation to the limit of vanishing shear rates, from which the model will provide the estimation of the dynamic yield stress.

Constant shear rate experiments are another commonly used rheological test. In these experiments, the fluid is subjected to a constant shear rate for a specified duration to achieve a desired level of shear strain. The resulting stress response is measured and plotted against the shear strain or time, providing valuable insights into the yielding

transition between the elastic solid and viscous liquid regimes. Figure 1.5 illustrates various methods for determining the yield stress in these experiments.
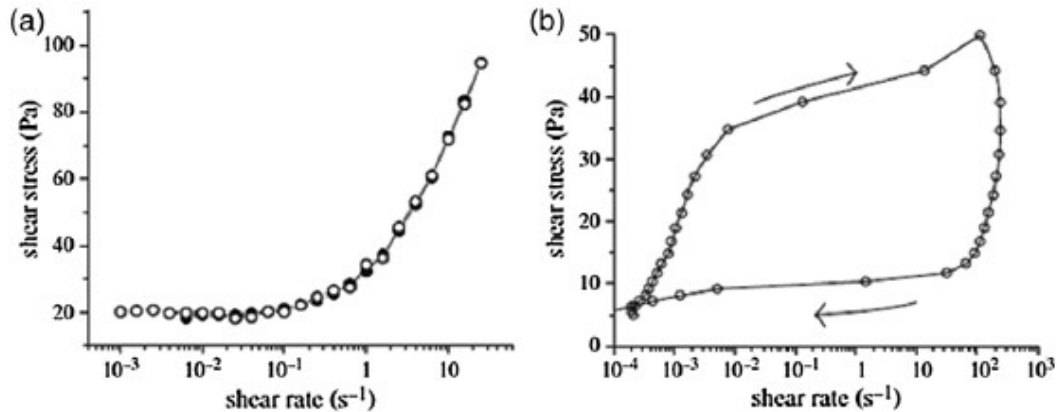
Figure 1.4 (a) The behavior of a 0.1% wt Carbopol microgel under increasing and decreasing shear rates shows a nonthixotropic response (filled circles, up; open circles, down). (b) Thixotropic response of a 10% wt bentonite solution under increasing and decreasing shear rate ramp.

Source: [2, 3]

However, in this study, the yield stress is defined as the point of departure from the region of linear elastic behavior. By comparing the approximate yield stress value obtained from the curve to the calculated yield stress, we can verify consistent yielding behavior across multiple systems, runs, and samples. This comparison will also enable us to assess whether the stress development within the sample follows a consistent pattern in each experiment, thereby enhancing our understanding of the behavior of the normal stresses.

To investigate the influence of flow history, intervals between constant rate experiments in this study will involve two different rest protocols. The first protocol will involve a 30-minute period of 0 shear rate ($\dot{\gamma} = 0.0s^{-1}$,) referred to as relaxation. This

rest period allows for the relaxation of internal shear and normal stresses, as well as

microstructural rearrangements, without any imposed conditions. In previous studies, the

residual stress observed when setting the shear rate to zero was utilized to determine the

yield stress.
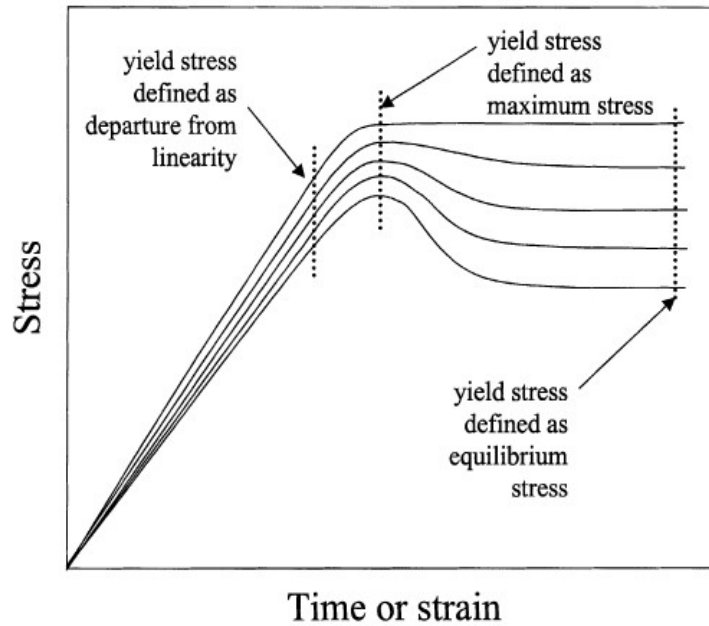
Figure 1.5 Typical start-up response of "yield-stress" materials during constant shear rate experiments, with various definitions of determining the yield stress.

Source: [22]

However, it has been determined that the residual stress obtained from these experiments

is significantly smaller than the dynamic yield stress determined by shear rate ramp

experiments [2]. Furthermore, it has been observed that the residual stress in these

experiments is influenced by the imposed shear rate, highlighting the dependence on test

history [24]. As part of the second protocol, a state of zero shear stress ($\tau = 0$ Pa), referred

to as recovery, will be imposed. The behavior of shear and normal stresses, as well as

strain, will be studied during this interval and in subsequent constant rate experiments.

Immediately after each constant shear rate experiment, the instrument will be instructed to return to a position where it maintains a state of zero shear stress, and it will remain in this position for approximately 30 minutes.

It is well known that different flow conditions can lead to varied measurements of the yield stress[2, 3]. While this work does not specifically aim to compare yield stress measurements, it is a critical point in yield stress rheology. Dynamic oscillatory shear measurements offer valuable insights into the viscoelastic behavior of the fluid. In this technique, a sinusoidal shear strain is applied to the fluid, and the stress response is recorded by measuring the dynamic moduli. The point at which the two moduli intersect is regarded as the yield point, indicating the transition of the material from a solid-like to a fluid-like state. In the low strain amplitude region (SAOS), which is often considered the linear regime, the stress response exhibits a sinusoidal pattern independent of the strain amplitude [25]. In the nonlinear regime, characterized by higher strain amplitudes, the stress response deviates from a sinusoidal pattern. LAOS (Large Amplitude Oscillatory Shear) experiments have demonstrated that at high frequencies, the stress response becomes more complex and requires advanced analytical techniques for evaluation [26]. It has been observed that yield stress estimations in this regime can be inaccurate due to complicated effects of the frequency ramp protocol. Additionally, the dependence of the stress response on both the applied frequency and harmonic response of the stress or strain may not align with the observations from other steady-state shear experiments. [2, 25, 27]. Creep experiments involve applying a constant shear stress and monitoring the corresponding strain response. Below the yield stress, the strain approaches a constant value, indicating the fluid behaves as an elastic solid. Above the

yield stress, the strain increases linearly with time resulting in flow like a viscous liquid. This test gives a calculation of the static yield stress. The difference in reaching a constant value of strain from linearly increasing strain is accompanied by a distinct change in viscosity, a phenomenon known as viscosity bifurcation [2], and can give reliable measurements of the static yield stress. However, it is important to note that measurements obtained through this technique often exhibit a dependence on flow history and may experience a phenomenon known as "delayed yielding" in very long test durations, where no flow is detected until the material eventually yields [2].

While there is no universal model that encompasses all these different flow conditions, there have been several models developed to represent their general flow behavior. The Bingham model for viscoelastic fluids was first introduced by Eugene Bingham in 1916 [28] and presents the simplest model that describes the rheological behavior for yield stress fluids in shear flows

$$\sigma < \tau_y \ \longrightarrow \ \dot{\gamma} = 0, \tag{1.13}$$

$$\sigma \geq \tau_y \ \longrightarrow \ \sigma = \tau_y + \eta\dot{\gamma}, \tag{1.14}$$

where τ_y is the yield stress, and η is the so-called plastic viscosity, which is constant [2]. Equation (1.14) reinforces the notion that above the yield stress, the fluid exhibits Newtonian behavior, with a constant viscosity. Conversely, equation (1.13) suggests that under a constant shear rate, the fluid's viscosity remains unaffected. Rearranging equation (1.14) highlights that the viscosity of yield stress fluids is indeed shear rate-dependent,

$$\eta = \frac{\sigma}{\dot{\gamma}} - \frac{\tau_y}{\dot{\gamma}}, \quad \text{for } \sigma \geq \tau_y \tag{1.15}$$

$$\eta \to \infty, \quad \text{for } \sigma < \tau_y \tag{1.16}$$

further emphasizing that yield stress fluids are non-Newtonian with a non-constant viscosity that depends on the shear rate past the yield point as previously discussed. Herschel and Bulkley improved upon the Bingham model that has since become the more widely utilized model to represent the yielding behavior of yield stress fluids. The Herschel-Bulkley [29] model is,

$$\sigma = \tau_y + K\dot{\gamma}^n, \quad \sigma \geq \tau_y \tag{1.17}$$

where K is the consistency, and n is the shear thinning index, which describes the degree to which a material has shear thinning ($n<1$) or shear thickening ($n>1$) behavior [30]. It is important to note that by setting $n=1$, this becomes equivalent to the Bingham model in (1.13) and (1.14). The model is a more generalized as it allows some flexibility for fitting experimental data and can accurately represent the yield stress region $\tau \approx \tau_y$ at low shear rates, and shear-thinning behavior at large shear rates [2]. In modern rheology, the behavior of these fluids can be described simply by the elastoviscoplastic model proposed by Oldroyd [31],

$$\sigma = G\gamma, \quad \text{for } \sigma \leq \tau_y \tag{1.18}$$

$$\sigma = \tau_y + K\dot{\gamma}^n, \quad \text{for } \sigma \geq \tau_y \tag{1.19}$$

that combines the Herschel-Bulkley model (1.17) with linear relationship between the shear stress, shear strain and shear modulus (1.5) that describes Hookean elastic solid behavior at low shear stresses prior to yielding.

1.4 Von Mises Yielding

For more complicated flows, the simple models described above must be generalized. The state of stress in a fluid is represented by the total stress tensor, $\vec{\vec{\pi}}$, made up of nine components that give information on the state of stress at any point in the fluid, and it is well established that the stress tensor is symmetric for most fluids [8]. The total stress tensor includes two contributions: an isotonic part that involves thermodynamic pressure, and a part that originates from fluid deformation,

$$\vec{\vec{\pi}} = p\vec{\vec{\delta}} + \vec{\vec{\tau}} \tag{1.20}$$

where p is the thermodynamic pressure, $\vec{\vec{\delta}}$ is the identity tensor and is symmetric, and $\vec{\vec{\tau}}$ is the (symmetric) extra stress tensor. Since only unidirectional shear flow is considered here, the extra stress tensor simplifies to

$$\vec{\vec{\tau}} = \begin{pmatrix} \tau_{11} & \tau_{12} & 0 \\ \tau_{21} & \tau_{22} & 0 \\ 0 & 0 & \tau_{33} \end{pmatrix}. \tag{1.21}$$

From this, the well-known definitions of the shear stress and the first and second normal stress differences are simply[8, 32, 33],

$$\sigma = \tau_{12} = \tau_{21}, \tag{1.22}$$

$$N_1 = \tau_{11} - \tau_{22}, \tag{1.23}$$

$$N_2 = \tau_{22} - \tau_{33}. \tag{1.24}$$

The most used criterion for determining the yield stress is the von Mises criteria,

$$\sqrt{\text{II}_{\tau'}} \geq \tau_y \tag{1.25}$$

where,

$$\text{II}_{\tau'} = \frac{1}{2}\left(\vec{\vec{\tau}}' : \vec{\vec{\tau}}'\right) \tag{1.26}$$

is the second invariant of the deviatoric stress tensor,[23]

$$\vec{\vec{\tau}}' = \vec{\vec{\tau}} - \frac{tr\left(\vec{\vec{\tau}}\right)}{3}\vec{\vec{\delta}}. \tag{1.27}$$

For simple shear flow, the von Mises yielding criteria is given by,

$$\sqrt{\text{II}_{\tau'}} = \sqrt{\sigma^2 + \frac{(N_1^2 + 2N_1N_2 + N_2^2)}{3}} \geq \tau_y \tag{1.28}$$

and is comprised of contributions from both the shear stress and normal stress differences. However, the elastoviscoplastic models in (1.18) and (1.19) imply that $N_1 = N_2 = 0$, so that $\sqrt{II_{\tau'}} = \sigma$.
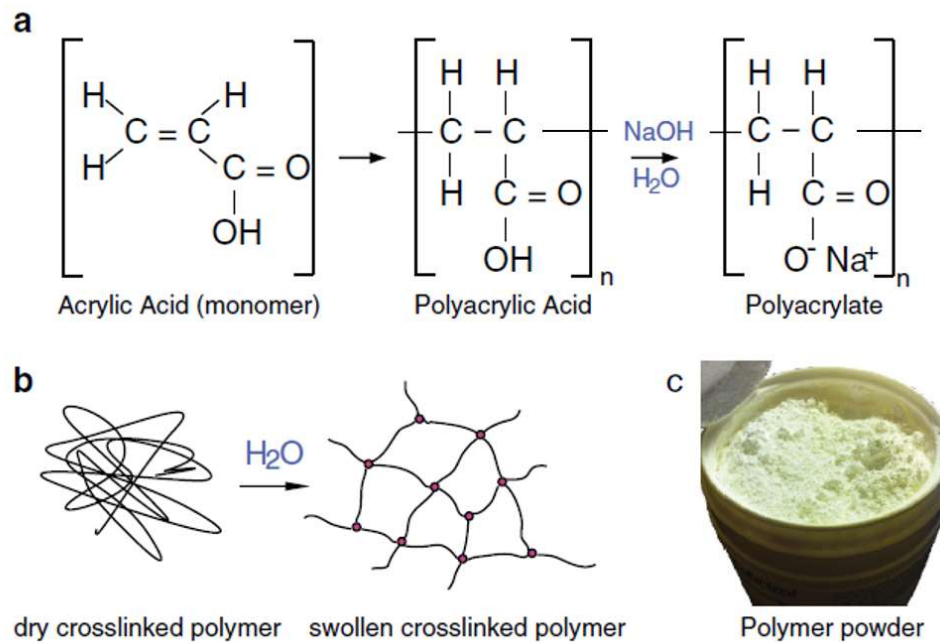
1.5 Carbopol

Figure 1.6 (a) Chemical reaction of (poly)acrylic acid with NaOH; (b) dry cross-linked polymer becomes hydrated and swells; (c) Carbopol powder prior to synthesis.

Source: [4]

Carbopol 940 is a high molecular weight, crosslinked polyacrylic acid $(C_2H_3COOH)n$ polymer (Figure 1.6). It is three-dimensional network that forms a colloidal dispersion with particles that vary in diameter based on solution concentration [23, 34-36]. Typical network structures contain between 1450 – 3300 [37, 38] monomer units between crosslinks with single chains reported to have molecular weights ranging from 104,000

[37] – 5 million g/mol [39], meaning the highly crosslinked network structure can weigh up to 4.5 billion g/mol[40]. Varying the concentration of the Carbopol solution also results in a range of reported viscosities, from 19,000 – 60,000 cPs[41, 42]. Carbopol is considered a model yield stress fluid as its steady state viscoelastic behavior is well-represented by the Herschel-Bulkley equation representing ideal yield stress and power-law shear thinning behavior [35, 36, 43]. It is widely accepted that the rheological properties of Carbopol dispersions stems from the microstructure deformation under various flow conditions [34-36, 43-46]. At low stresses, the Carbopol behaves as a viscoelastic solid until the yield stress is exceeded, upon which it flows like a viscous liquid [36, 43, 47]. The microstructure first deforms elastically, with chains stretching without moving past one another that return to their original state upon the removal of the force. With higher applied stresses, the colloidal particles begin to move past one another as chains breakdown, decreasing the number of entanglements in the system. Given enough time at rest the network beings rebuilding to a form that resembles that of the undeformed material [43]. The varying conditions of the rest period is the focus here, as there is evidence that subsequent experiments on a Carbopol sample can simultaneously result in both reproducible and chaotic behavior of stresses during shearing flows [23].

1.6 Normal Stresses in Yield Stress Fluids

To understand why the normal stresses are being investigated here, previous works must be evaluated to understand their shortcomings or lack of clarity regarding the information they present. There are numerous previous studies done studying carbopol microgels, primarily because they present model yield stress fluid properties that allow for simplistic

modelling and evaluation of rheological phenomena. However, many works either neglect the study of normal stress differences, include little information on their behavior or neglect a key mechanical artifact known as axial compliance.

Carbopol's rheological properties have been studied extensively over the last 50 years. Many studies report measurements of the shear stress and rheological properties, and some do include considerations of the normal stress. But most leave out any measurements of the normal stress differences [2, 4, 34, 35, 43, 44], despite being a key component of stress development in complex fluids. This has changed in the last 20 years with some researchers turning their focus to the behavior of normal stresses under shear flow, and Carbopol being a perfect candidate for study. Multiple reviews on Carbopol rheology have been written that critique the lack of inclusion of normal stress differences, saying they cannot be ignored and doing so ignores a key component of complex fluid rheology [23, 35, 36, 43].

Despite best efforts there are still shortcomings that appear repeatedly in papers on the subject. Many authors that report normal stress difference measurements seem to typically report only a limited number of datasets regarding normal stress behavior[14, 15, 48, 49]. This eliminates the possibility of assessing the reproducibility of normal stress behavior in these systems, as even more recent work has demonstrated a nonreproducible nature of their behavior in Carbopol microgels [23]. The lack of repeat runs also suggests that even though care may be taken to ensure an ideally relaxed state prior to making measurements, there is no assessment of the impact of test history on the normal stress in subsequent flow experiments. Microstructural rearrangements between measuring intervals require sufficient time or conditions to return to their initial or near

initial state so that subsequent tests return accurate results. The recent work from Venerus et. al.[23] found that a 30 minute relaxation window leads to chaotic behavior of normal stress behavior in a Carbopol yield stress fluid. Other studies have noted that normal stresses may require hours of relaxation time between shearing events for sufficient microstructural rebuilding [50-52]. This work aims to improve understanding of the impact of test history and a recovery period on the behavior of normal stress differences.

For research that has considered normal stress behavior, there is also some disagreement on the sign of N_1 and N_2. For the case of N_1, it is well known that for polymer liquids that $N_1 > 0$, and most literature has reported data that supports this [14, 15, 48]. However there are some reported values of $N_1 < 0$ [53] or $N_1 \sim 0$ [23] for constant shear rate and oscillatory shear experiments of yield stress fluids. For the case of N_2, there have been no reports of $N_2 > 0$, meaning that current available works report $N_2 < 0$ or $N_1 - N_2 > 0$[48, 49], and there is only one reported work with the opposite case of $N_1 - N_2 < 0$ [53]. The range of disagreements may stem from the fact that most of these works only consider one type of experiment, whereas allowing for multiple tests may provide further insight into the true behavior of the normal stresses, and aid in the development of yield stress fluid models.

CHAPTER 2

EXPERIMENTAL

In this chapter, the techniques for preparing Carbopol samples will be discussed, along with the test parameters and procedures used in the experiments conducted in this work. Since two different instruments were employed to investigate rheological phenomena, certain sections will provide methods applicable to both instruments, while others will specify the instrument used.

2.1 Sample Preparation

Samples of 1 wt. % Carbopol 940 (Lubrizol Corp.) were prepared in a manner like that described in Venerus et.al.[23] Carbopol powder was collected after passing through a 40mm mesh sieve to ensure uniform powder particle distribution. It was then dissolved in de-ionized water and stirred for 60 minutes, after which a dilute sodium hydroxide (NaOH) solution was added to neutralize the polyacrylic acid solution. The neutralized polymer network then absorbs water and swells to form the final gel. The gel was then removed from the stir plate and stirred by hand for approximately 5 minutes until it displayed uniform characteristics. It was then transferred to a centrifuge tube and centrifuged at 3500 rpm for 10 minutes to eliminate air bubbles trapped in the microgel. The pH of the gel was measured and found to be pH $\approx$ 7, which typically produces gels with the same microstructure. The sample was allowed to rest for at least 24 hours prior to testing to allow for any residual stresses from the centrifugation process to dissipate.

2.2 Rheometry

There are numerous techniques and tools at the disposal of rheologists for studying rheological phenomena in fluids. Understanding the operational principles and measurement modes of rotational rheometers is crucial. In this study, two commonly employed rheometers are utilized. The first is a strain-controlled rheometer (RMS800), which applies a controlled strain to the sample. The second is a stress-controlled rheometer (MCR301), which maintains a constant stress on the sample. The key distinction between the two rheometers lies in the placement of the transducer within the instrument. In strain-controlled rheometers, the transducer is located in the upper stationary plate, and it measures the deformations caused by the rotation of the bottom plate. These rheometers receive a signal specifying the desired strain level, and based on this input, the required rotational speed is determined. The resulting torque and force experienced by the transducer are measured to characterize the sample's rheological properties. In contrast, stress-controlled rheometers have the transducer situated in the upper rotating plate, which applies deformation to the sample resting on a stationary bottom plate. These instruments operate using a constant feedback loop, where an angular velocity is applied, and the resulting torque is continuously measured. Corrections are made based on the measured torque to maintain the desired stress conditions throughout the test.

There are multiple types of tools and test geometries available for rheological tests. The most common are parallel-plate, cone-plate, and concentric cylinders. Here only cone-plate and parallel-plates will be discussed, as concentric cylinders were not used in this work. Figure 2.1 shows a schematic of parallel-plate and cone-plate

geometries used to make rheological measurements. These geometries rely on the principle of torsional flow, where the material is subjected to shear stress resulting from the rotational motion of one plate with respect to the other. In parallel-plate experiments, a fluid is placed between two disks of identical radius R at a known gap width H, such that $R \gg H$ (Figure 2.1, left). The upper plate rotates with a known angular velocity, Ω to apply a constant shearing force across the surface area of the sample. This allows for measurements of the shear strain experienced by the sample, and measurements of rheological properties such as viscosity, and yield stress. An important note about parallel-plate measurements is that the applied shear rate is dependent on radial position. Boundary conditions state that the velocity $v_\theta = 0$ at $z = 0$, and $v_\theta = r\Omega$ at $z = H$, and results in the following relationship shear strain rate,

$$\dot{\gamma} = \dot{\gamma}_R \frac{r}{R} \tag{2.1}$$

where $\dot{\gamma}_R$ is the strain rate at the outer edge of the parallel plate, and has the following relationship,[8]

$$\dot{\gamma}_R = \frac{R\Omega}{H} \tag{2.2}$$

The system also records the axial force, F, exerted on the upper plate during these experiments, which will be needed to make calculations of the normal stress coefficients N_1 and N_2.
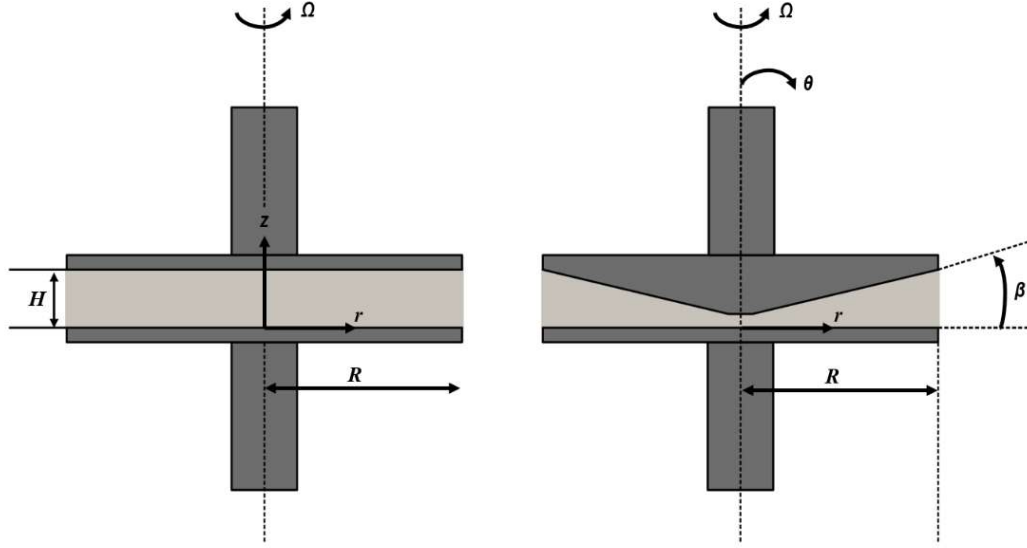
Figure 2.1 Schematic of parallel-plate (left) and cone-plate (right) test geometries.

Knowing this allows us to make measurements of the shear stress and normal stress difference $N_1 - N_2$, which is done by relating the torque, M, experienced by the moving plate to maintain the desired shear rate or angular velocity, and is calculated using the known relations [8, 33]

$$\sigma = \frac{3}{4}\left(\frac{2M}{\pi R^3}\right) + \frac{\gamma_R}{4}\frac{d\left(\frac{2M}{\pi R^3}\right)}{d\gamma_R} \tag{2.3}$$

$$N_1 - N_2 = \left(\frac{2F}{\pi R^2}\right) + \frac{\gamma_R}{2}\frac{d\left(\frac{2F}{\pi R^2}\right)}{d\gamma_R}. \tag{2.4}$$

However, the more preferred testing geometry for rheological experiments is the cone plate setup (Figure 2.1, right) Its popularity stems from the fact that it eliminates the problem of radial dependence of the shear rate that occurs in parallel-plate flow [8]. In

cone-plate flow the shear rate is constant throughout the entire sample for small angles of

β, meaning the material will yield homogenously throughout the sample [30]. With this,

the shear rate is instead simply

$$\dot{\gamma} = \frac{\Omega}{\beta}.\tag{2.5}$$

Like parallel plate experiments, the instrument measures torque and axial force so that the

shear stress and first normal stress difference N_1 can be determined with the following

equations [8, 33],

$$\sigma = \frac{3M}{2\pi R^3}\tag{2.6}$$

$$N_1 = \frac{2F}{\pi R^2}.\tag{2.7}$$

The above techniques have an associated error propagation that stems from instrument

tolerances and is described in detail in Section 2.6.

2.3 Test Instruments

During the experiment, two rheometers, namely the RMS800 (Rheometrics Inc) from and

the MCR301 (Anton Paar,) were utilized. Both rheometers were equipped with 50mm

diameter cone-plate and parallel-plate fixtures. To minimize slip during testing, 400 grit

sandpaper was affixed to the test fixtures. The selection of the surface roughness was

based on the general guideline that it should be comparable to the microstructural size of

the sample under investigation [2]. For the RMS800 parallel-plate experiments, a 50mm diameter was used with a 2.0mm gap (H = 2.0mm). For cone-plate experiments on the RMS800, a 50mm diameter plate with a cone angle (β) of 0.1 rad and a truncation distance of 60μm were employed. For the MCR301 parallel-plate experiments, a 50mm diameter plate was used with a 2.0mm gap (H = 2.0mm). For cone-plate experiments on the MCR301, a 50mm diameter plate with a cone angle (β) of 0.105 rad and a truncation distance of 500μm were employed. Figure 2.2 provides images of the above instruments, along with examples of the test geometries with the sandpaper-adhered surfaces.
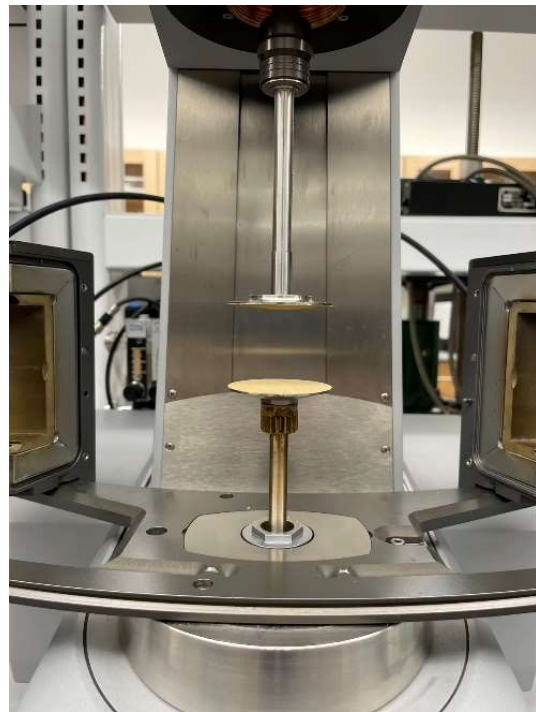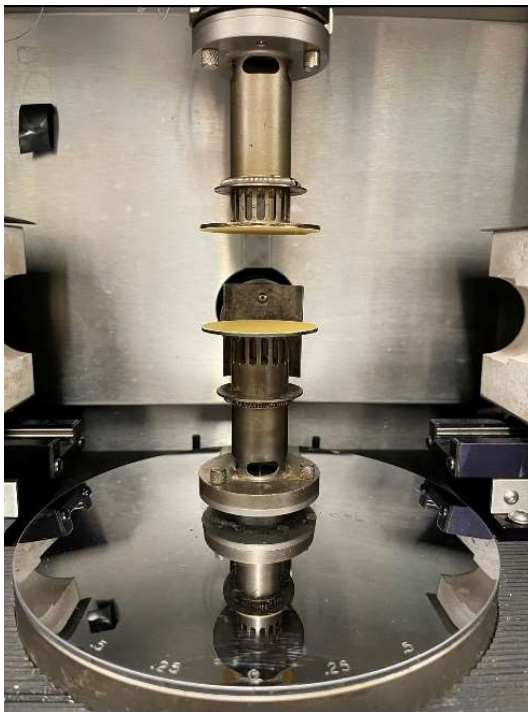
Figure 2.2 Rheometric RMS800 strain-controlled rheometer (top left); Anton Paar MCR301 Stress controlled rheometer (top right); sandpaper adhered parallel-plate geometry on RMS800 (bottom left); sandpaper adhered cone-plate geometry on MCR301 (bottom right.)

2.4 Sample Loading and Pre-shear

All rheological measurements were conducted at room temperature $22 \pm 1°C$ in an enclosed environment with a water-saturated sponge to minimize evaporation. Carbopol was loaded onto the lower plate and subjected to a controlled squeeze to ensure uniform filling of the gap in both cone-plate and parallel-plate geometries. On the RMS800 the squeezing procedure is conducted manually. The upper plate was lowered over the course of approximately 500 seconds to the final test position. For the cone-plate geometry the position was a truncation distance of 60 μm, and for the parallel plate geometry the gap was 2.0mm. The squeeze procedure for the MCR301 is similar but is instead automatically controlled by the Anton Paar Rheometrics software. The upper plate was lowered from a 5.0mm starting position to the test position over the course of 400s: 500 μm truncation for cone plate tests, and 2.0mm for parallel plate tests. On both instruments, after squeezing the edge of the sample was trimmed of excess material and allowed to stand for approximately 30 minutes to allow for the relaxation of residual stresses. Next, a pre-shear conditioning test was run on all samples. It consists of the application of alternating constant shear rates in the following sequence: $\dot{\gamma} = 1.0, -1.0,$ 1.0, -1.0 s^{-1} for 100s each, after which the edge of the sample was gently repaired and allowed to rest for 30 minutes to allow residual stresses to relax prior to rheological tests.

2.5 Rheological Tests

The first rheological test conducted on all Carbopol samples was an oscillatory frequency sweep experiment to make measurements of the shear (G) and complex moduli (G^*) , and dynamic moduli (G' and G''.) For cone-plate experiments, the applied angular

frequency is increased logarithmically from ω=0.1 rad/s to 100 rad/s, at a strain amplitude of 0.005. For parallel plate experiments, the applied angular frequency was increased logarithmically from ω=0.1 rad/s to 100 rad/s, at a strain amplitude of 0.003.

A shear rate ramp test was conducted on samples using the Anton Paar MCR 301. The shear rate was increased logarithmically from $0.004s^1$ to $10s^{-1}$, then decreased logarithmically from $10s^{-1}$ to $0.004s^{-1}$. Each shear rate was run long enough to induce a shear strain $\gamma = 4$ on the sample. This demonstrates the materials dependence only upon shear rate and not the magnitude of shear. Rate ramp experiments also verify the nonthixotropic nature of the Carbopol samples, and to provide repeat experiments to reliably determine the yield stress when fitting with the Herschel-Bulkley model.

On the RMS800 constant shear rate experiments were conducted on Carbopol samples using both cone-plate and parallel-plate geometries to collect a large number of data sets to study the behavior of the normal stresses. Samples were subjected to a constant shear rate of $\dot{\gamma} = 0.1^{-s}$ for 40s to reach a final strain of $\gamma = 4$. Each subsequent run was sheared in the opposite direction (clockwise versus counterclockwise, or positive versus negative shear direction) to eliminate any directional dependency that may appear in the results. It is important to note that the normal force (F) and torque (M) were manually set to zero between each constant rate experiment. Prior to the onset of shear flow, the dials that measure these quantities were reset to zero, so that uniform stress measurements were made for each experiment. The samples were then allowed to wait for 30 minutes so residual stresses could naturally relax prior to the start of the next test. Each loaded sample produced 5-6 runs before the Carbopol began to dry out or degrade

from repeat flow experiments. The shear and normal stress data were collected and analyzed to study their behavior.

On the MCR301 constant shear rate experiments were conducted in a similar manner. However, a larger range of shear rates were evaluated that aid in developing a more detailed picture of the rheological behavior. Shear rates of $0.01s^{-1}$, $0.03s^{-1}$, $0.1s^{-1}$, $0.3s^{-1}$, $1.0s^{-1}$, and $3.0s^{-1}$ were used with the cone and plate geometry. For parallel plate, shear rates of $0.01s^{-1}$, $0.1s^{-1}$, and $1.0s^{-1}$ were evaluated. Each shear rate was run for a prescribed amount of time that would result in a final shear strain of $\gamma = 4$. This was again done in alternating directions to eliminate any directional dependence that may appear in the results. In contrast to the RMS800, here the normal force (F) and torque (M) are set to zero only prior to the first constant rate experiment. Between constant rate and recovery intervals, the Rheometrics software does not return measurement values to zero, and therefore the data is adjusted to acquire accurate results. This is done by subtracting the final value (either shear or normal stress) of the previous test from the first value of the "current" test to determine the zero point for that experiment. These samples were not set to relax 30 minutes. Immediately upon completion of the constant rate experiment, the Carbopol was subjected to a recovery interval where $\tau = 0Pa$. During this time the strain and normal stresses were allowed to recover in a controlled manner, whose results are shown in chapter 3.

2.6 Transducer Axial Compliance

A mechanical consideration that impacts the reliability of rheological measurements of the normal stress differences is transducer axial compliance [23, 54-57]. Simply put, it is

related to the rheometer's transducer stiffness. The compliance of the transducer can influence the measurement of rheological parameters, such as viscosity, the yield stress, and shear and normal stresses. Therefore, it is essential to account for the axial compliance of the transducer when conducting rheological experiments to ensure accurate and precise results. Because the normal stresses that are being investigated are small, it is important to eliminate any potential artifacts that may develop during shear flows. When normal stresses are generated in a complex fluid, there is a small axial displacement of the fixture attached to the transducer. This displacement in turn generates flows in the radial direction, which then further generates additional normal stresses [23]. Avoiding this is therefore critical to ensure that only the normal stresses that develop due to shear deformation are measured. To achieve this, it is required that the transducer has an axial stiffness large enough to eliminate this concern [23, 55]. This is accomplished by ensuring that the transducer response time is small compared to the relaxation time of the material in question. Multiple studies discuss the impact of axial compliance on mechanical measurements and have presented criteria that allow for avoiding the impact of transducer axial compliance. It has been shown [23, 54-57] that the relationship to create ideal conditions for cone-plate and parallel are represented by,

$$\frac{\lambda_A}{\lambda_M} = \frac{6\pi GR}{K_A \beta^3} \tag{2.8}$$

$$\frac{\lambda_A}{\lambda_M} = \frac{3\pi GR}{2K_A (H/R)^3} \tag{2.9}$$

where λ_A is the axial response time of the transducer, λ_M is the relaxation time of the material, G is the shear modulus, R is the radius of the plate, K_A is the axial stiffness, β is the cone angle, and (H/R) is the ratio of the gap to plate radius. The suggested criteria to satisfy the above relations to avoid compliance problems is $\lambda_A/\lambda_M \ll 1$ [23], and the above relations suggest that β or (H/R) must be large, along with the axial stiffness. It has been demonstrated that using large cone angles improves the consistency of normal stress measurements when compared to small cone angles [23]. This is an important consideration that is made here to eliminate any experimental artifacts, giving confidence that measurements are reliable and accurate when evaluating the impact of the recovery period. Care was taken to ensure that the test geometries were used that satisfy (2.1) and (2.2), meet the criteria of $\lambda_A/\lambda_M \ll 1$. The response time ratios for the geometries employed here are shown below in Table 2.1, using a value of $G = 421$ as determined below in section 3.1, where it is apparent that artifacts due to transducer axial compliance do not play a role in the normal stress measurements recorded in this work.

Table 2.1 Transducer Axial Compliance Response Ratios of the RMS800 and MCR301 Rheometers

	RMS800 λ_A/λ_M ($K_A = 4\text{N} / \text{μm}$)	MCR301 λ_A/λ_M ($K_A = 2\text{N} / \text{μm}$)
Cone -Plate	0.05	0.09
Parallel -Plate	0.02	0.05

2.7 Error Propagation

In any measurement, there is inevitably some degree of error stemming from instrument tolerance and sensitivity. In the case of rotational rheometers, errors arise from the sensitivity of the transducer torque and normal force, as well as deviations in the sample radius from the plate radius. To quantify the uncertainties that may arise in measured quantities, such as shear and normal stresses, error propagation formulas are employed. Equations (2.3), (2.4), (2.6), and (2.7) are used to calculate the shear and normal stresses, and they incorporate an associated error based on the variables measured in rheological experiments. The tolerances of these variables are summarized in Table 2.2.

Table 2.2 Instrument Tolerances for the RMS800 and MCR301 Used in Error
Propagation Calculations

Source of Error	RMS800	MCR301
Torque (ΔM)	2×10^{-4} N·m	2×10^{-7} N·m
Normal Force (ΔF)	2×10^{-2} N·m	2×10^{-3} N·m
Plate Radius (ΔR)	1 mm	1 mm

The equations for error propagation for the shear stress and normal stresses are,

$$\frac{\Delta \sigma}{\sigma} = \sqrt{\left(\frac{\Delta M}{M}\right)^2 + \left(3\frac{\Delta R}{R}\right)^2} \tag{2.10}$$

$$\frac{\Delta N}{N} = \sqrt{\left(\frac{\Delta F}{F}\right)^2 + \left(2\frac{\Delta R}{R}\right)^2} \tag{2.11}$$

2.8 Rheometer Consistency Tests

To ensure the consistency and comparability of results between the RMS800 and
MCR301 rheometers, a calibrated Newtonian viscosity standard was tested on both
instruments to function as a reference material with known rheological properties. A
shear rate ramp test was conducted on the samples, with shear rates increasing from $\dot{\gamma} = 0.1s^{-1}$ to $\dot{\gamma} = 10s^{-1}$, the results of which are shown in Figure 2.3. This plot
demonstrates the consistency and agreement between the instruments when measuring
the viscosity standard above $\dot{\gamma} = 0.5s^{-1}$. Below this shear rate there is disagreement
between data due to the resolution limitation of the transducer on the RMS800. This
comparison ensures the reliability and accuracy of the rheological measurements
performed using the two rheometers throughout the experiment.
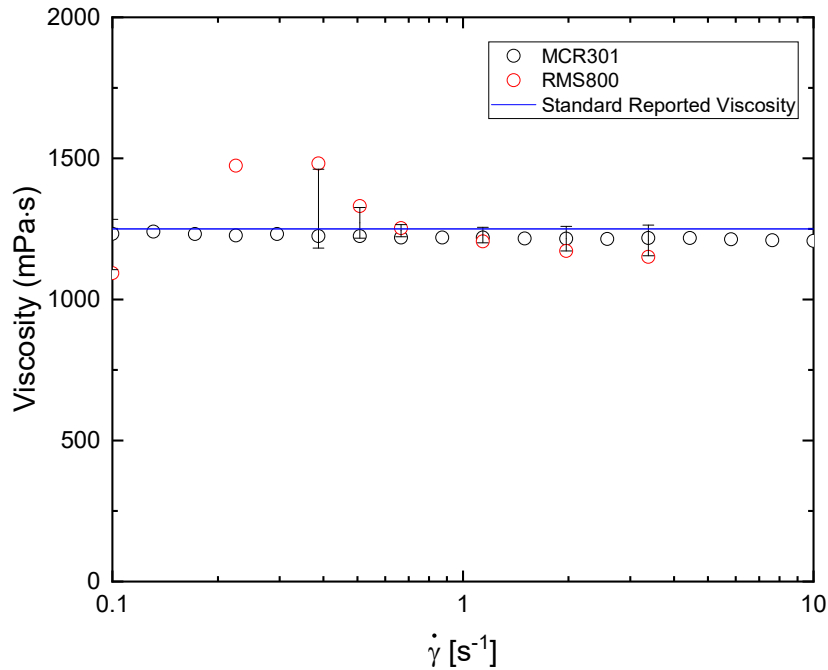
Figure 2.3 Viscosity calibration tests on the MCR301 (black circles) and RMS800 (red
circles), with reported viscosity from the calibration standard (blue line) at 22.6 °C. Error
bars represent the standard deviation between the measurements.

In addition to the viscosity test, a single sample of Carbopol was evaluated on each instrument on the same day. A pre-shear test was conducted with the following sequence $\dot{\gamma}$ = 1.0, -1.0, 1.0, -1.0s^{-1} for 100s each, with stress responses from these tests shown in Figure 2.4. Both samples then had edge fractures repaired and were allowed to rest for 30 minutes. The stress response from each instrument is identical, indicating the samples were conditioned appropriately. Next, a small amplitude oscillatory shear experiment was run with angular frequencies that increased logarithmically from 0.1 rad/s to 100 rad/s at a strain amplitude of 0.005.
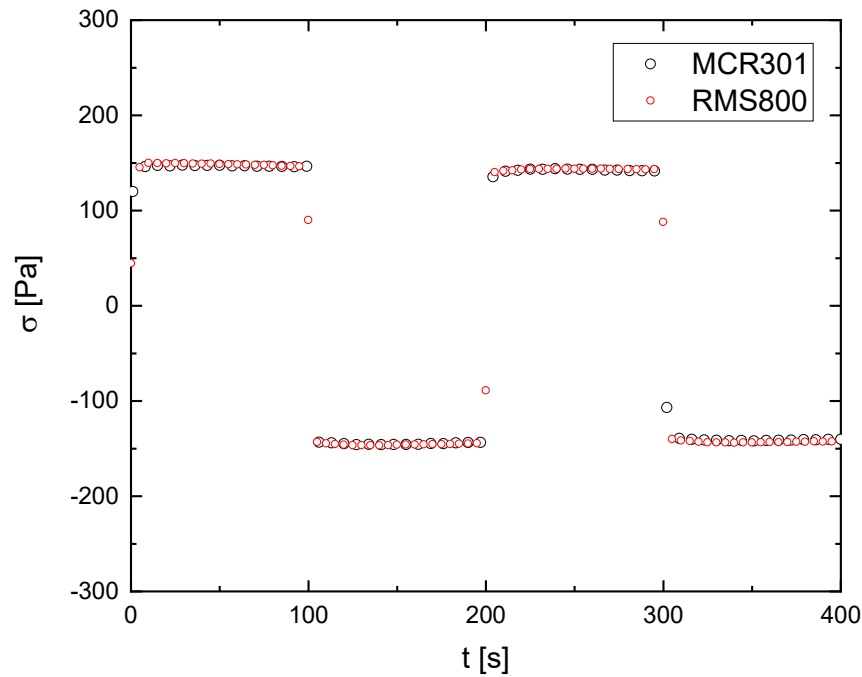
Figure 2.4 Pre-shear agreement tests on the MCR301 and RMS800.

These results are shown in Figure 2.5, where again there is good agreement of the dynamic moduli measured on each instrument, giving information that both samples possess the same fluid properties in both low and high frequency regimes.
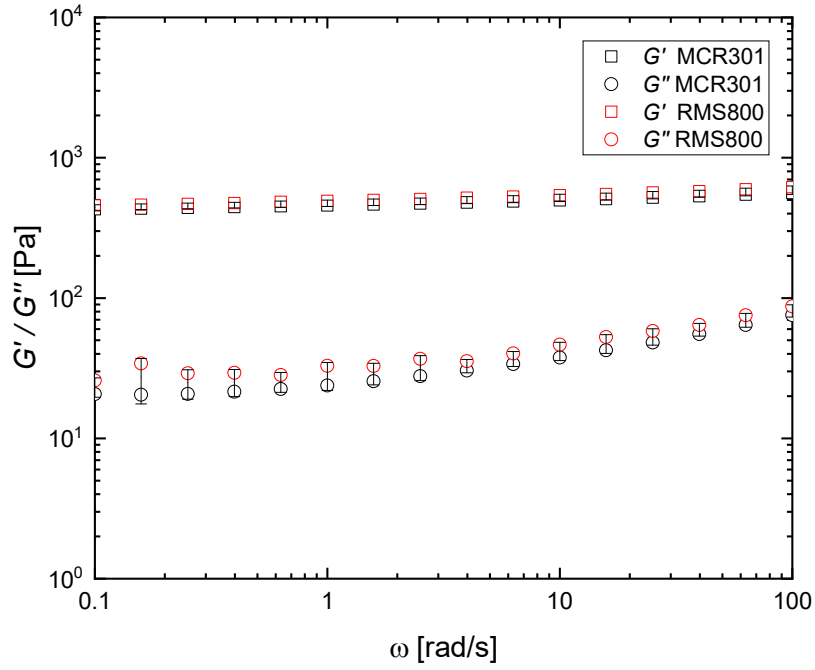
Figure 2.5 Dynamic moduli G' ($\square$) and G'' ($\circ$) versus angular frequency, ω, on the MCR301 (black symbols) and RMS800 (red symbols.)

Finally, both samples were subjected to 4 constant shear rate experiments with $\dot{\gamma} = 0.1s^{-1}$ for 40 seconds to a strain of 4 (Figure 2.6). The results compiled from the above tests give confidence that measurements made between instruments are comparable and reliable when the comparison between relaxation and recovery is considered.
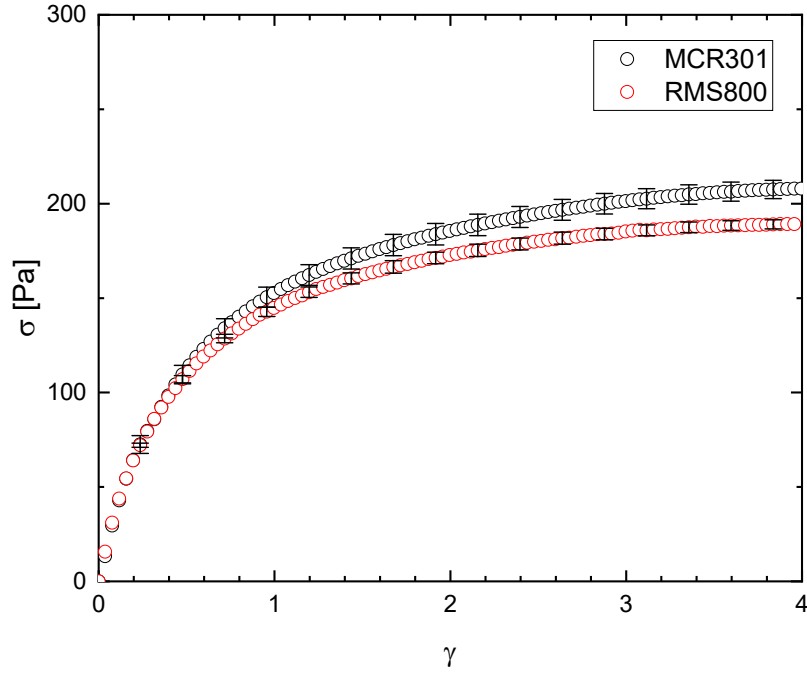
Figure 2.6 Constant shear rate experiments conducted on the MCR301 and Rheometrics RMS800 with $\dot{\gamma} = 0.1 s^{-1}$ for 40. The average of 3 runs from each instrument are shown. Error bars represent standard deviations of measurements.

CHAPTER 3

RESULTS AND DISCUSSION

3.1 Results and Discussion

Results of rheological experiments are presented here, beginning with squeezing profiles. During squeezing the normal force was monitored as the gap decreased from 5.0mm to 0.5mm in cone-plate tests, and from 5.0mm to 2.0mm in parallel-plate tests. Results are shown in Figure 3.1, where ten squeezing profiles are plotted from each test geometry. The response reaches a maximum when the final test position is reached, then decreases as excess fluid is trimmed and the sample is let to rest for ~30 minutes so residual stresses can relax. It is important to note here that normal force never returns to a state of 0 N when the squeezing procedure is complete, even after the rest period. This is an expected result and is like others discussed in the literature [50-52].

The average of 10 SAOS experiments using cone and plate geometry are shown in Figure 3.2. The curves show an expected profile for gel-like viscoelastic behavior with $G' > G''$ across the range of test frequencies. Using the approximation from (1.12), G' is used to determine the shear modulus of the carbopol sample. The value is taken at $\omega = 0.1$ rad/s so that $G = G'(\omega) = G'(0.1 \text{ rad/s})$ [7, 23], giving $G = 421$ Pa, which is in agreement with similar Carbopol 940 solutions from previous works [15, 48]. Like the validation measurements, these measurements confirm that all samples evaluated have the same microstructural and viscoelastic characteristics. At all measured frequencies, the storage modulus dominates measurements indicating that the material is behaving as a viscoelastic solid.
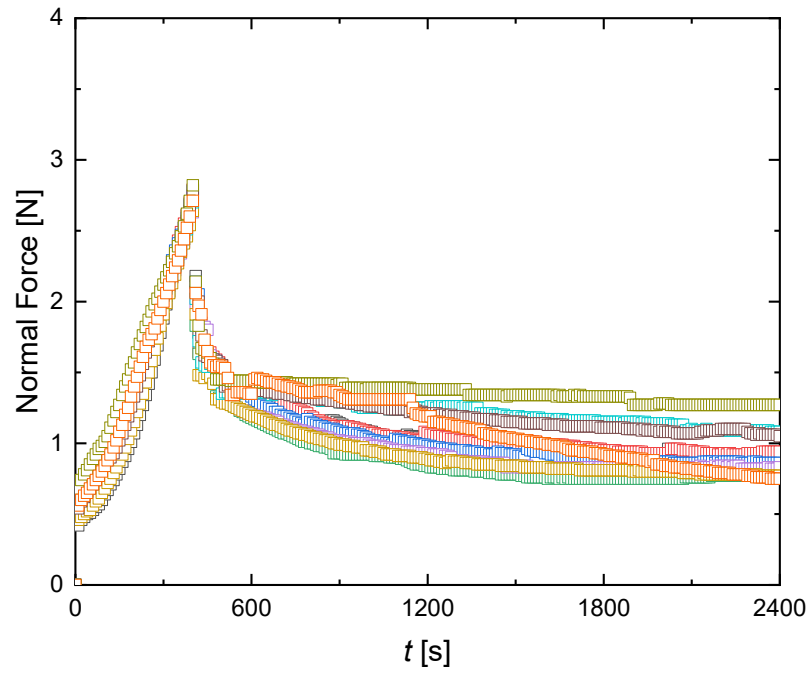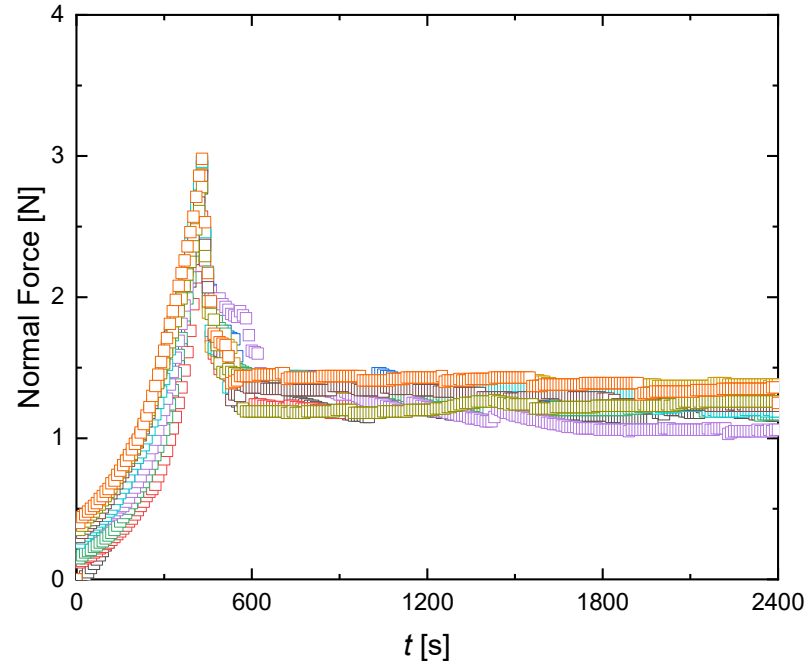
Figure 3.1 Squeezing and rest profile of Carbopol in cone-plate (top) and parallel plate (bottom) geometries on the MCR. Different colors represent different runs.
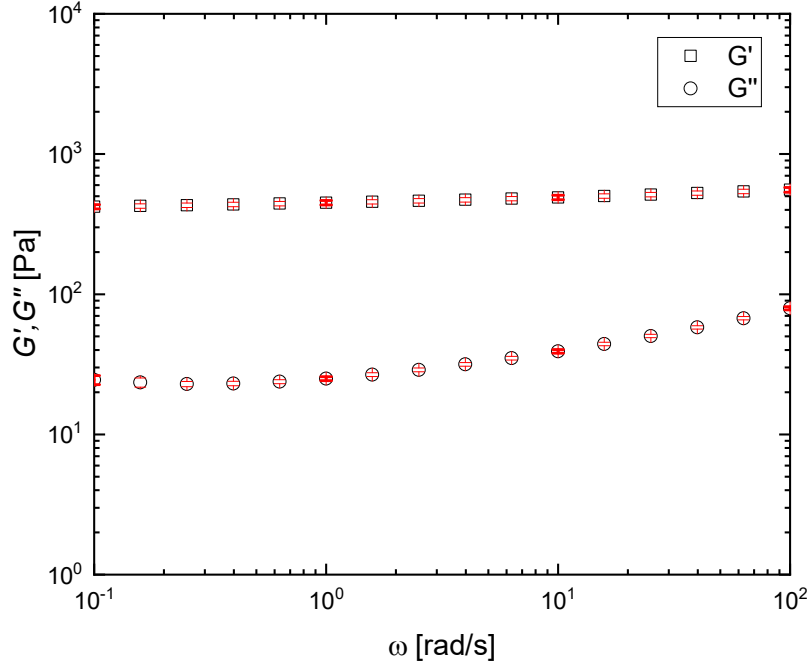
Figure 3.2 Dynamic moduli G' ($\square$) and G'' ($\circ$) versus angular frequency ω for 10 runs of Carbopol 940. Red error bars indicate standard deviations of measured values.

Next the results of the shear rate ramp are shown in Figure 3.3 and Figure 3.4. The average of 10 repeat runs using cone and plate geometry are presented, where the lack of hysteresis in Fig. 3.3 indicates the presence of simple yield stress fluid behavior [3, 5, 23, 58]. The Bulkley-Herschel model in (1.17) was used to fit the data from the decreasing strain rate ramp and used to determine the dynamic yield stress of the microgel. Fitting and extrapolation of the data to $\dot{\gamma} = 0$ s^{-1} leads to the determination of the yield stress to be $\tau_y = 92$ Pa, which is similar to other results discussed in the literature [36]. Figure 3.4 is the average N_1 data for 10 shear rate ramp tests. There is only some hysteresis present, but there is good agreement of the normal stress behavior in both the increasing and decreasing shear rate ramps. While this is not typically a method considered to model simple yield stress fluid behavior, it does suggest that perhaps like

the shear stress, the normal stresses may be independent of time and has some

dependence on the shear rate.
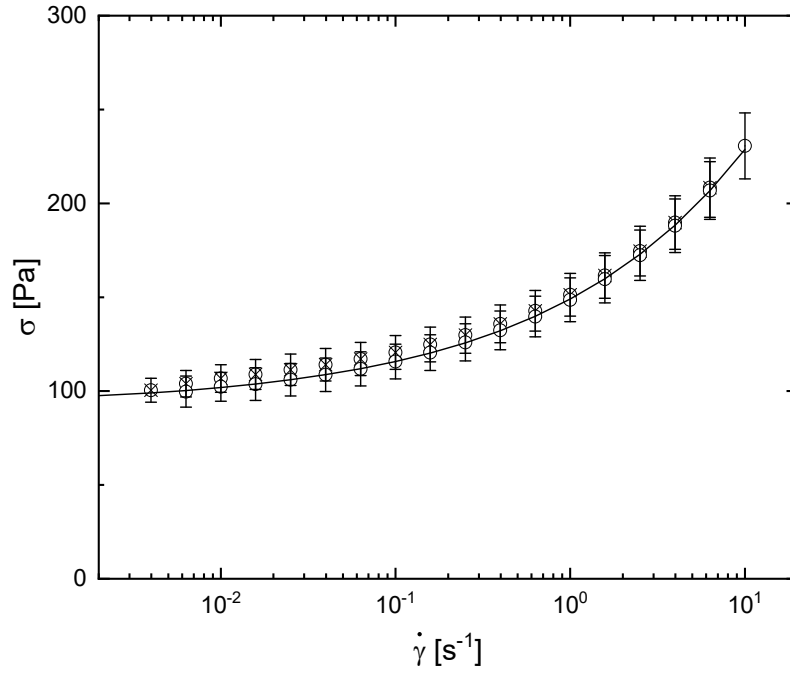
Figure 3.3 Flow curve for Carbopol 940 microgel using cone-pate geometry of shear stress ($\dot{\gamma}$ increasing $\otimes$, $\dot{\gamma}$ decreasing $\circ$) versus shear rate. The solid line is a fit of equation (1.19) with $\tau_y = 92$ Pa, $K = 57$ Pa·s^n, and $n = 0.38$. Error bars represent standard deviations of measured values.
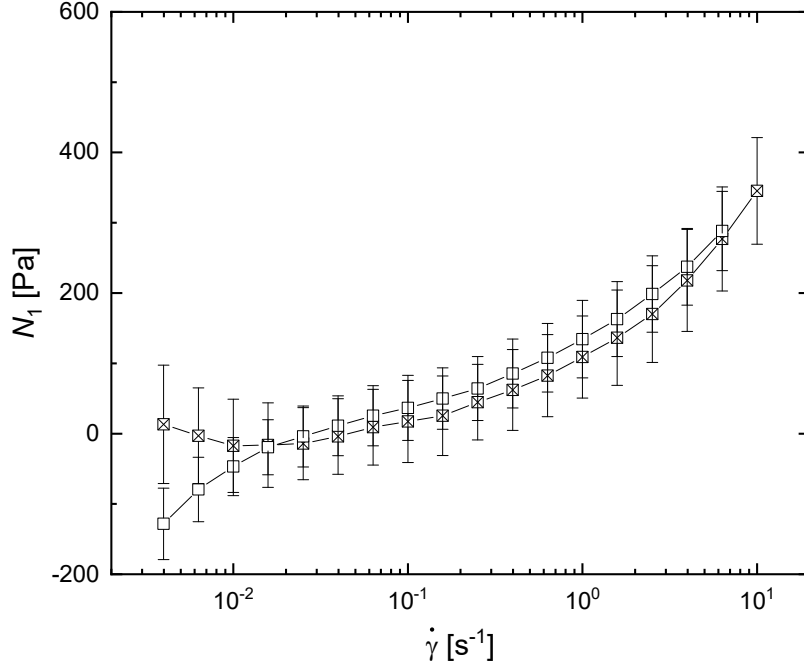
Figure 3.4 Flow curve for Carbopol 940 microgel using cone-pate geometry of N_1 ($\dot{\gamma}$ increasing ⊠, $\dot{\gamma}$ decreasing ☐) versus shear rate. Error bars represent standard deviations of measured values.

Constant rate experiments for $\dot{\gamma} = 0.1 s^{-1}$ following relaxation are shown in

Figure 3.5. Shear stress and N_1 data are plotted for 34 runs on the RMS800 with cone-

plate geometry; σ and N_1 measurements were made simultaneously. Initially the shear

stress shows a linear dependence on strain until yielding (γ ~ 0.1) after which the stress

approaches a steady state value (~200 Pa here) for the remainder of the experiment, like

other results [23, 35, 45]. Shear stresses demonstrate good reproducibility for all runs,

while N_1 progresses in a clearly chaotic manner. This result agrees with similar recent

work by Venerus et.al. [23]. Initially, N_1 measurements are small compared to the values

of the shear stress prior to the onset of viscous flow. This would suggest that the normal

stresses do not significantly contribute to the flow behavior of the fluid prior to yielding,

which is again consistent with previous results [23, 48]. The average of N_1 results from

these experiments indicate that $N_1 < 0$, which agrees with other results found in the

literature [23]. Monitoring during relaxation also gives some insight into the behavior of

residual normal stresses that exist after cessation of the shear flow, where results are

shown in Figure 3.6. The shear stress relaxes in a viscoelastic manner, approaching a

steady state value of residual stress known as the relaxation modulus described by the

Maxwell Model [7, 59]. However, N_1 shows a decrease briefly at the start of the interval,

then once again grows chaotically, recovering some of its previous magnitude in

agreement with the literature [50], and it suggested to be attributed to the restricting of

the microgel while at rest [60]. These results further indicate that normal stresses may

never fully relax in this period and may impact the normal stress response in subsequent

flows.

Constant rate ($\dot{\gamma} = 0.1 s^{-1}$) experiments following recovery intervals for cone-

plate and parallel plate flows are shown in Figures 3.7 and 3.8, respectively. There is a

noticeable change in the magnitude of the steady state shear stress and behavior of the

normal stresses from relaxation experiments. These plots are qualitatively similar,

indicating good reproducibility and similar flow behavior between test geometries.

Difference in the normal stress behavior in parallel plate experiments is due to the

measurement of $N_1 - N_2$, rather than solely N_1. Again, at low strain values ($\gamma \sim 0.1$) the

shear stress demonstrates a linear relationship with strain with an approach to a constant

value of stress (~125 Pa) for the remainder of the experiment after yielding, a decrease

from ~200 Pa from relaxation experiments (Figure 3.5.)
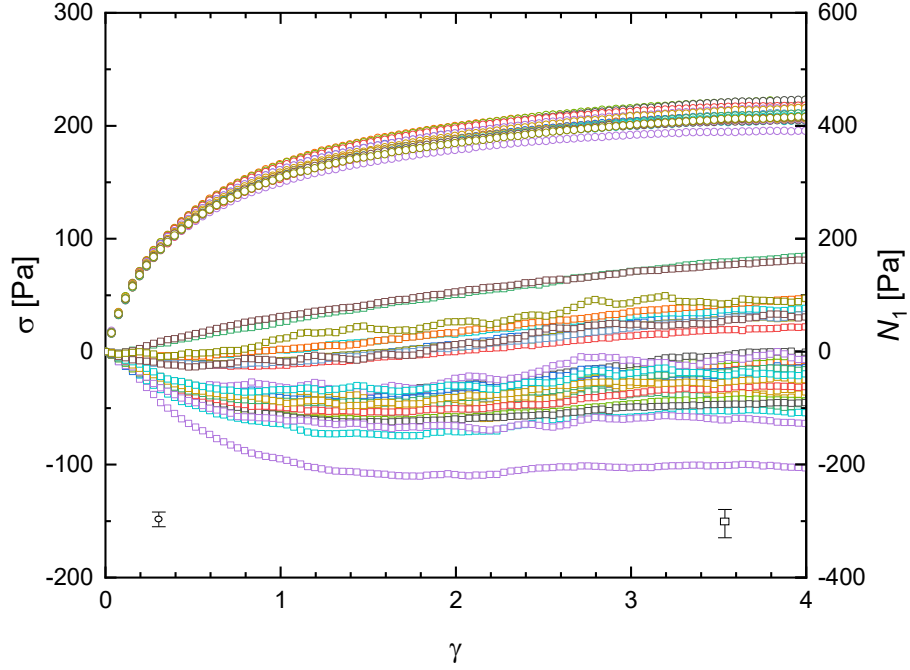
Figure 3.5 Shear stress σ (○) and N_1 (□) from constant shear rate ($\dot{\gamma} = 0.1s^{-1}$) experiments after a 30-minute relaxation period conducted on the RMS800 with cone-plate geometry. Error bars represent estimated error in computed quantities.
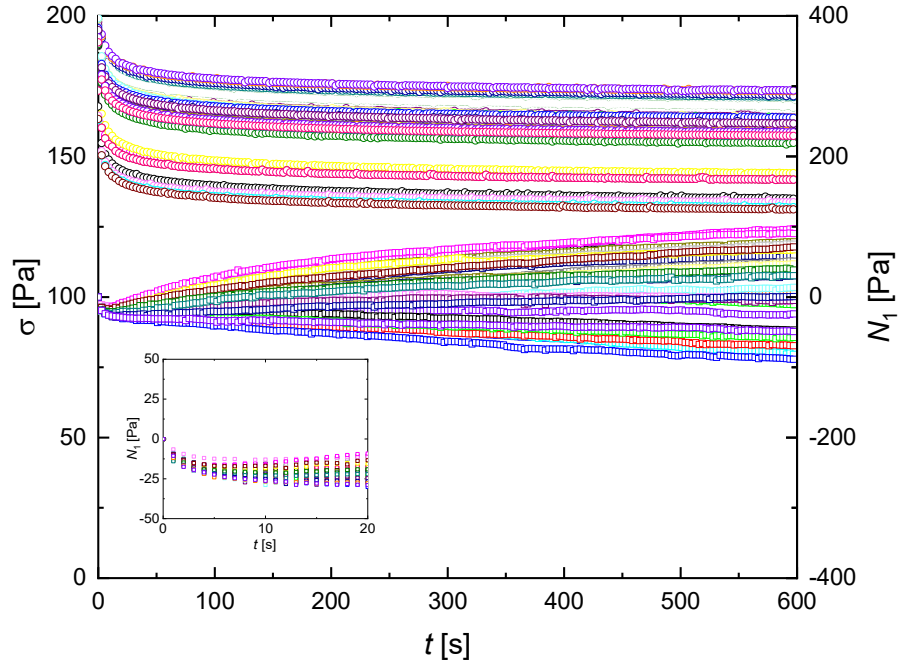
Figure 3.6 Shear stress σ (○) and N_1 (curves) during relaxation intervals after constant rate experiments on the RMS800 with cone-plate geometry. The inset show N_1 behavior at the start of the relaxation interval.
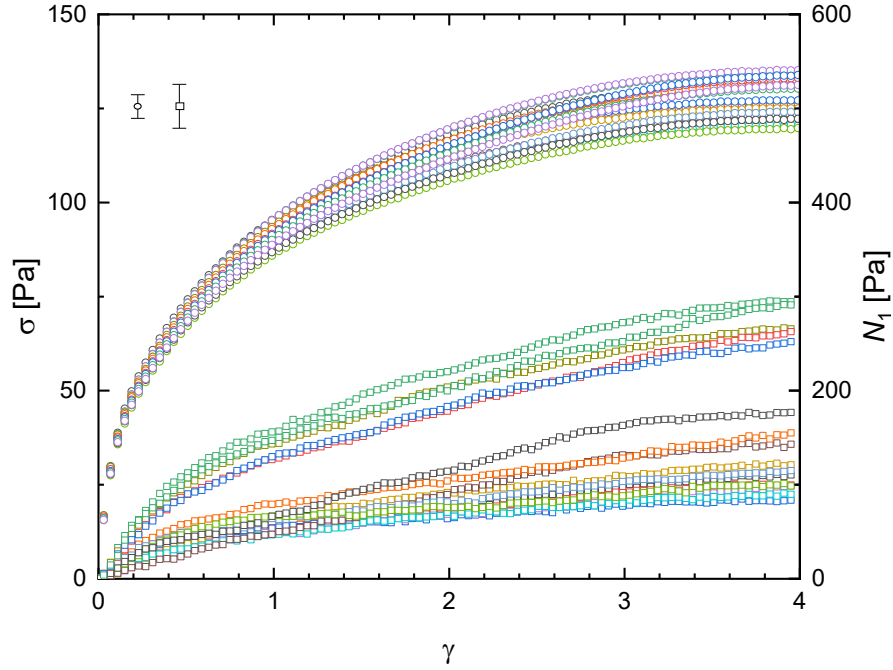
Figure 3.7 Shear stress σ (○) and N_1 (□) from constant shear rate ($\dot{\gamma} = 0.1s^{-1}$) experiments after a recovery period conducted on the MCR301 with cone-plate geometry. Error bars represent estimated error in computed quantities.

Figure 3.8 Corrected shear stress $2M/\pi R^2$ (○) and $N_1 - N_2$ (□) from constant shear rate ($\dot{\gamma} = 0.1s^{-1}$) experiments after a recovery period conducted on the MCR301 with parallel plate geometry (different color symbols.) Error bars represent estimated error in computed quantities.
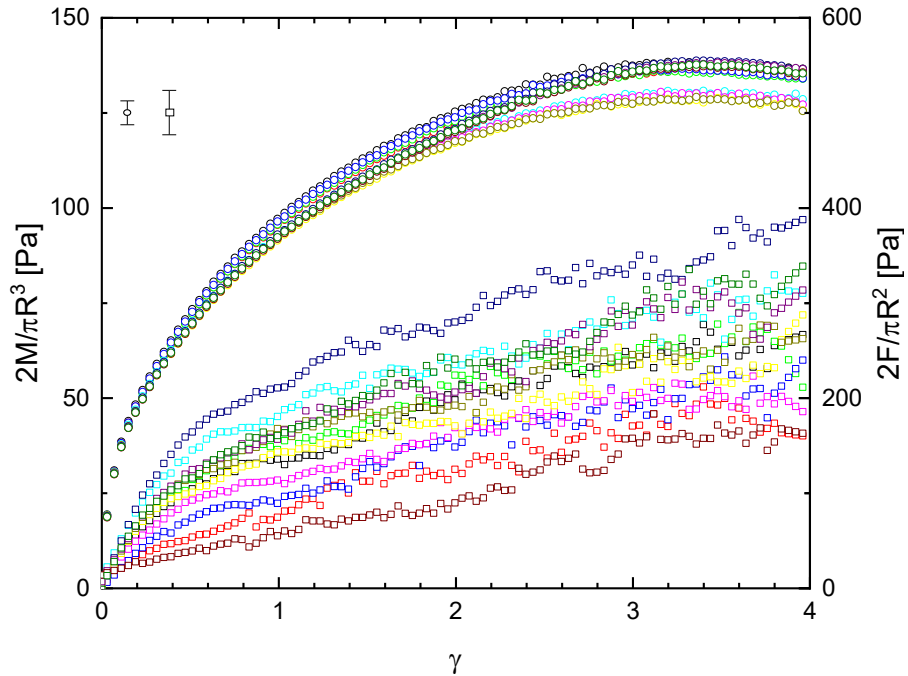
There is also a marked difference in the behavior of the first and second normal stresses. Where relaxation experiments suggest chaotic growth during shear flows, the recovery experiments demonstrate a more consistent growth pattern of the normal stresses. This may be indicative of a forced reorganization of the Carbopol microstructure during recovery. Because recovery intervals are characterized by returning the fluid to a state of zero stress, microstructural rearrangement that typically require time to relax are perhaps instead moved back into sate that resembles pre-yield conditions. These measurements find that $N_1 > 0$ and $N_1 - N_2 > 0$, meaning $N_2 < 0$. These averages of the shear and normal stresses in Figures 3.7 and 3.8 are shown in Figure 3.11. This is in agreement with both the established normal stress behavior for polymeric fluids [32, 33] and previous studies investigating normal stress differences in yield stress fluids [14, 15, 48, 49]. The results presented here are therefore believed to be accurate representations of the normal stress behavior during constant shear rate experiments. In addition, the comparison of the average σ and N_1 from relaxation and recovery experiments are shown in Figures 3.9 and 3.10. These plots show a clear impact on the stress behavior of the carbopol when subjected to the recovery period that results in a decrease of the magnitude of the shear stress and sign change for N_1 over the entire test range. This significant change in N_1 behavior raises a question of instrument performance. Such a stark difference may suggest that the rheometers may be incorrectly measuring the normal stress behavior during flow experiments. However, when referring to the supplemental material of Venerus et.al. [23], it is demonstrated that the instruments used in this work and their paper show good agreement and agree with the rheometer consistency tests conducted in this work. They also tested a common viscoelastic fluid (10%polystyrene in diethyl-

phthalate solution) that demonstrated reproducible shear and normal stress behavior, further indicating that the instruments are making measurements of the normal stresses accurately.

At this point it is important to discuss the importance of transducer compliance once again in rheological measurements. At shown in Table 2.1, care was taken to ensure that the response time ratios in this work satisfy the criteria of $\lambda_A/\lambda_M \ll 1$. This gives confidence that the findings here are accurate and reliable measurements of the normal stresses. When comparing our results to others, it is apparent that others may not have taken transducer compliance into account when making normal stress measurements [15, 48, 49, 53]. These results were calculated using very small cone angles with transducer stiffness of $K_A \sim 2$ N/μm that result in $\lambda_A/\lambda_M > 1$, meaning it is not evident that axial compliance concerns were considered, and their normal stress difference measurements may not be reliable. Others[14, 23], chose cone angles that were large enough to satisfy the criteria of $\lambda_A/\lambda_M \ll 1$.

Results from relaxation and recovery experiments were then plotted against the elastic prediction (1.18) and von Mises yielding criteria (1.28) in Figure 3.12. The plot shows that at low strain below the yield point ($\gamma \sim 0.1$), the stress growth is linear and in agreement with the elastic prediction and von Mises yielding criteria, indicating Hookean elastic behavior, as expected as N_1 and N_2 data are small in this region. After yielding the von Mises yielding shows a deviation from the observed measurements of σ, indicating that the growth of N_1 and N_2 impacts the fluid behavior greatly after the onset of yielding. This plot further emphasizes the impact of recovery intervals between constant shear flow

experiments, as the shear stress deviates from the elastic prediction at a lower value of

shear stress than that observed in relaxation experiments.
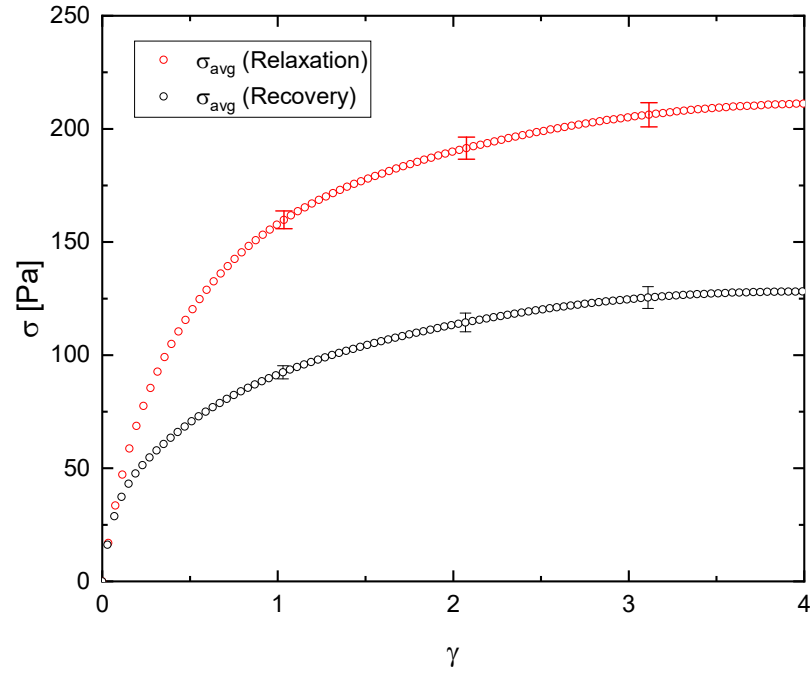
Figure 3.9 Average σ from relaxation (○) and recovery (○) experiments at $\dot{\gamma} = 0.1s^{-1}$ for 40s. Error bars represent standard deviations from measurements.
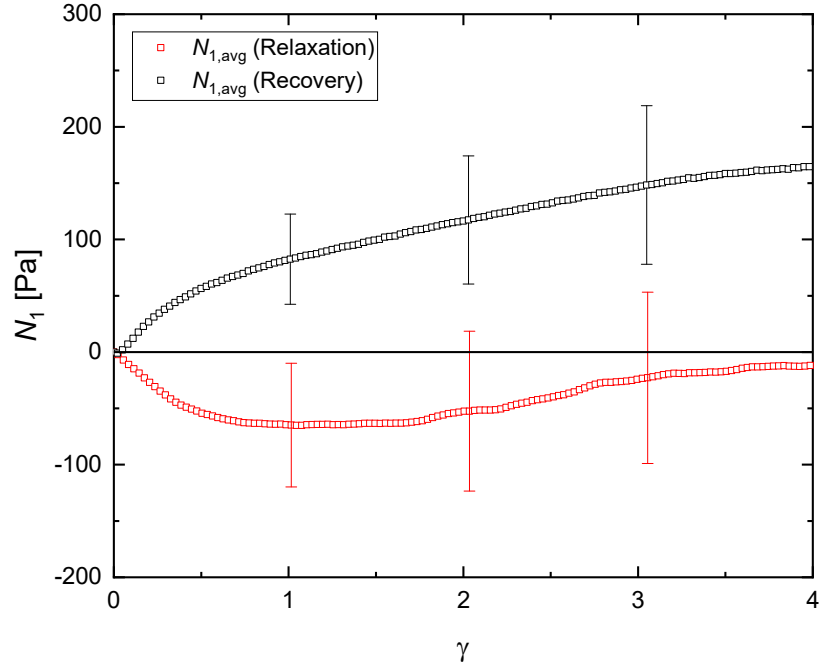
Figure 3.10 Average N_1 from relaxation ($\square$) and recovery ($\square$) experiments at $\dot{\gamma} = 0.1s^{-1}$. Error bars represent standard deviations from measurements.
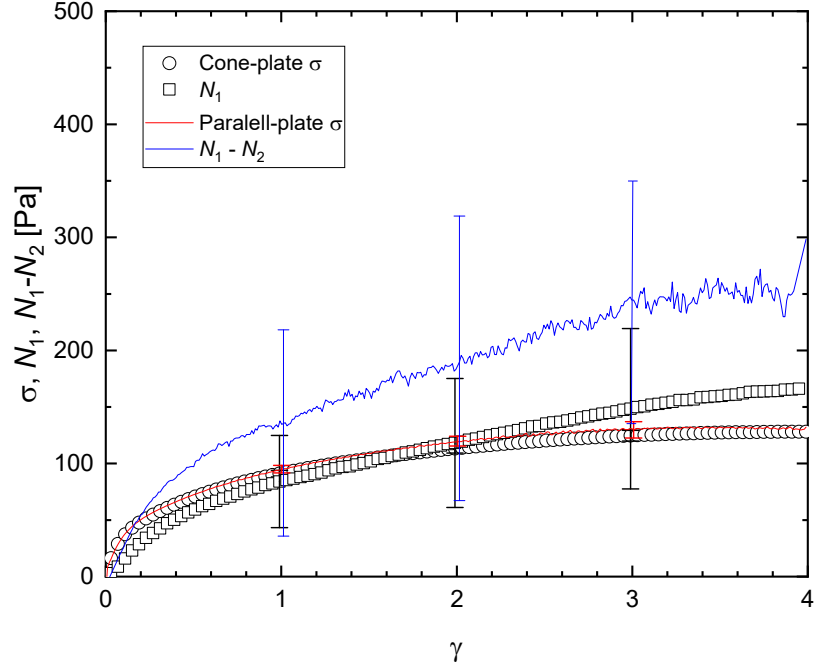
Figure 3.11 Average σ ($\circ$) and N_1 ($\square$) (black symbols) from Figure 3.6 and computed average σ (red curve) and $N_1 - N_2$ (blue line) from Figure 3.7. Error bars represent standard deviations from repeat experiments.
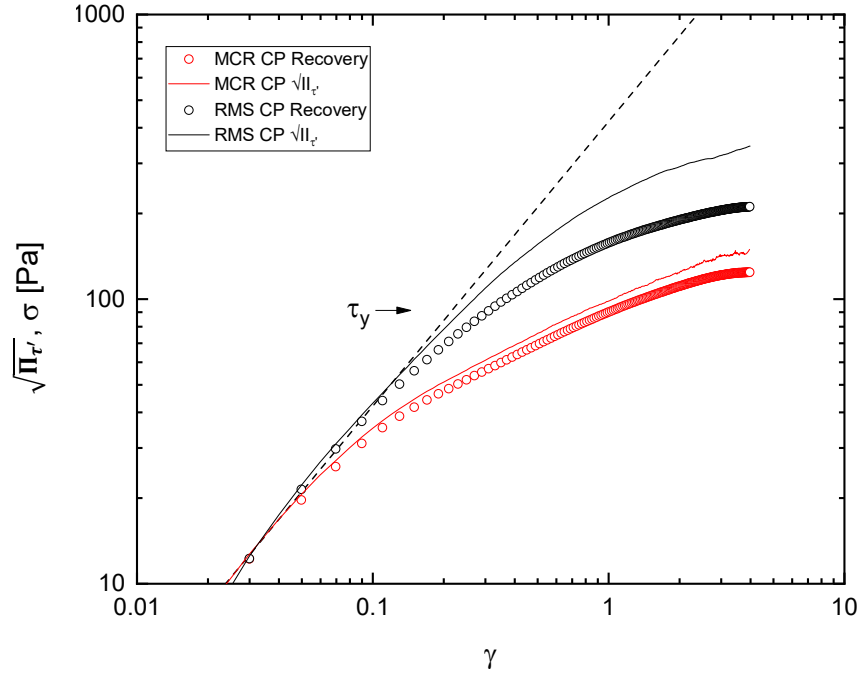
Figure 3.12 Shear stress σ (○) and $\sqrt{II_{\tau'}}$ (curves) versus strain γ for RMS800 cone-plate relaxation and MCR cone-plate and parallel-plate recovery experiments for shear rate $\dot{\gamma} = 0.1s^{-1}$. The dashed line is the linear elastic solid prediction (1.18) with G = 421 Pa; the arrow indicates the yield stress τ_y = 92 Pa obtained from Figure 3.3.

Recovery experiments were also conducted at a wider range of shear rates.

Results of individual shear rates are shown in Figures 3.13 – 3.19, and their average

stress response is plotted in Figure 3.20 along with the stress response from relaxation

experiments in Figure 3.5. There is a clear impact of shear rate on the stress response of

Carbopol, with the magnitude of the stress increasing with shear rate.

Figure 3.13 Shear stress σ ($\circ$) and N_1 ($\square$) from constant shear rate ($\dot{\gamma} = 0.01 s^{-1}$) experiments after a recovery period conducted on the MCR301 with cone-plate geometry. Error bars represent estimated error in computed quantities.
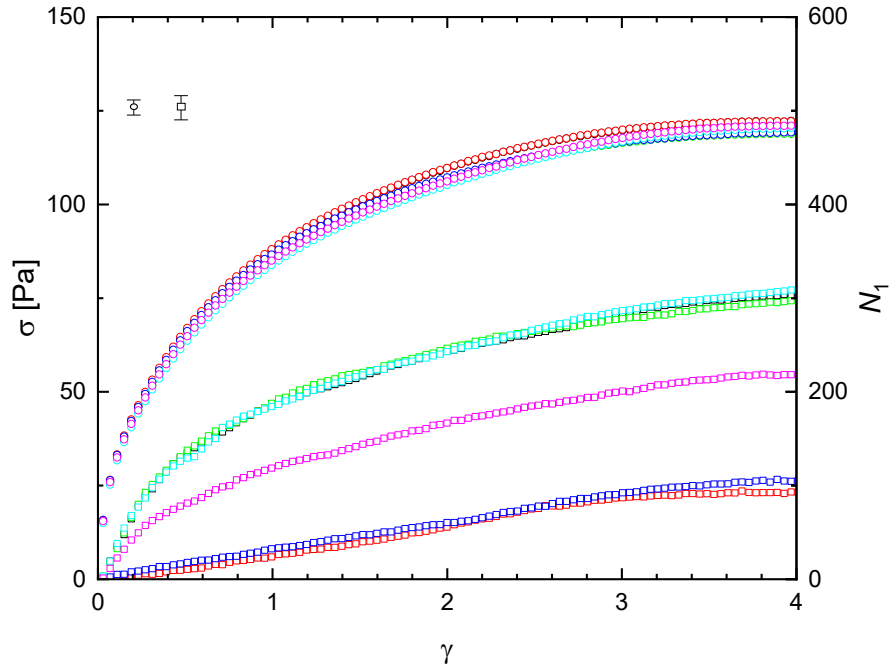
Figure 3.14 Shear stress σ ($\circ$) and N_1 ($\square$) from constant shear rate ($\dot{\gamma} = 0.03 s^{-1}$) experiments after a recovery period conducted on the MCR301 with cone-plate geometry. Error bars represent estimated error in computed quantities.
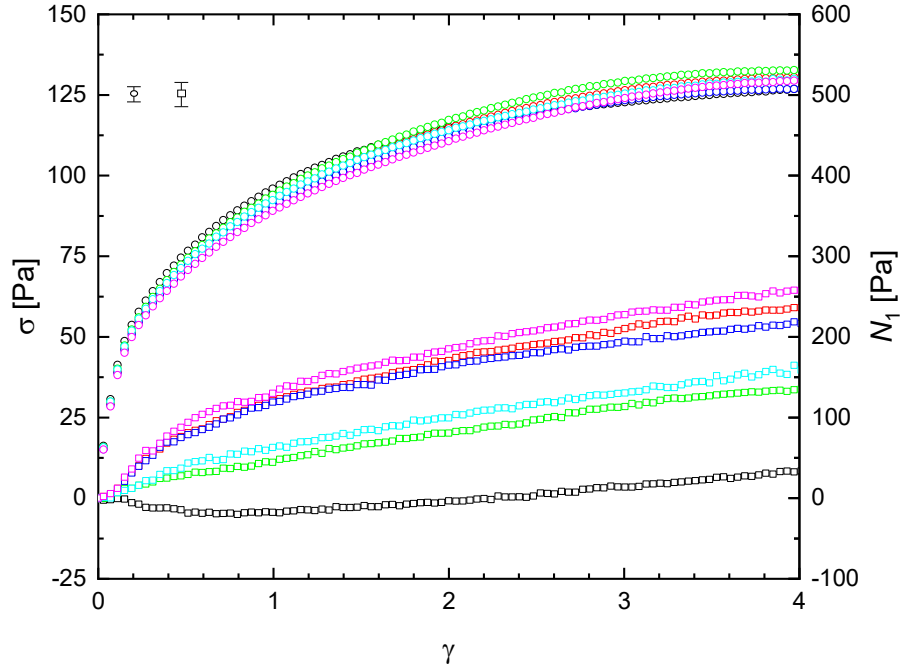
Figure 3.15 Shear stress σ ($\circ$) and N_1 ($\square$) from constant shear rate ($\dot{\gamma} = 0.3s^{-1}$) experiments after a recovery period conducted on the MCR301 with cone-plate geometry. Error bars represent estimated error in computed quantities.
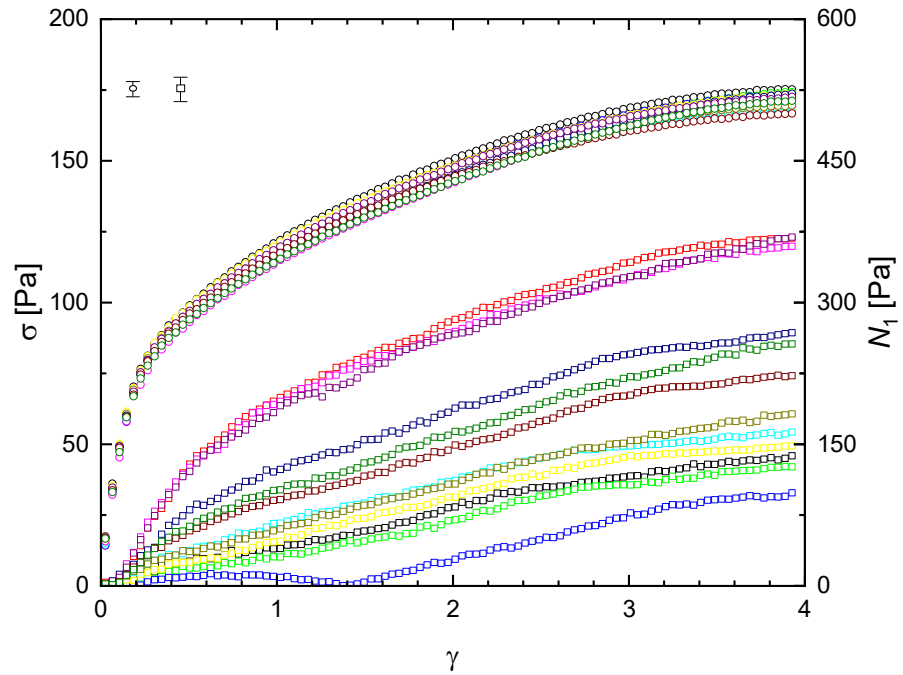
Figure 3.16 Shear stress σ ($\circ$) and N_1 ($\square$) from constant shear rate ($\dot{\gamma} = 1.0s^{-1}$) experiments after a recovery period conducted on the MCR301 with cone-plate geometry. Error bars represent estimated error in computed quantities.
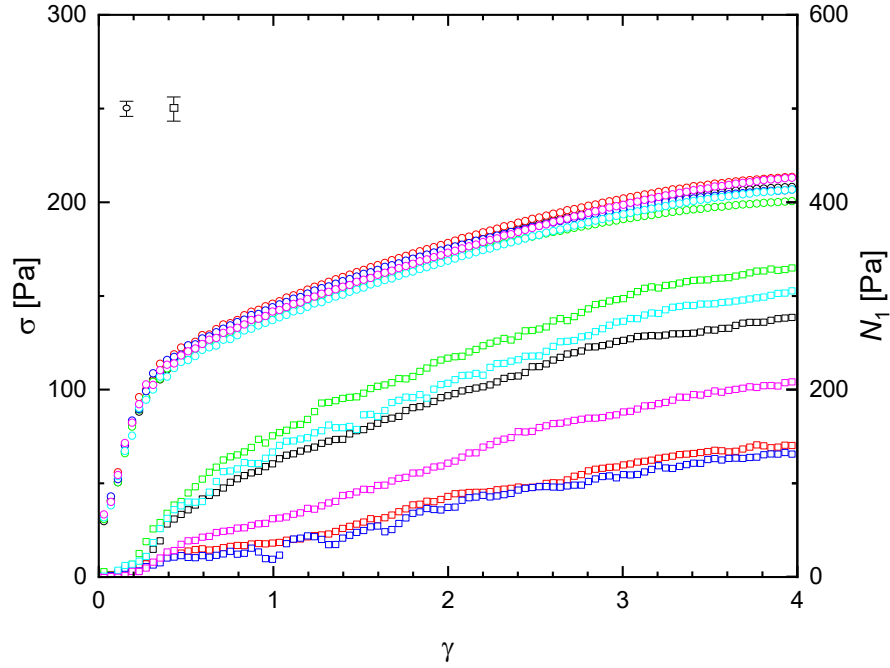
Figure 3.17 Shear stress σ ($\circ$) and N_1 ($\square$) from constant shear rate ($\dot{\gamma} = 3.0 s^{-1}$) experiments after a recovery period conducted on the MCR301 with cone-plate geometry. Error bars represent estimated error in computed quantities.
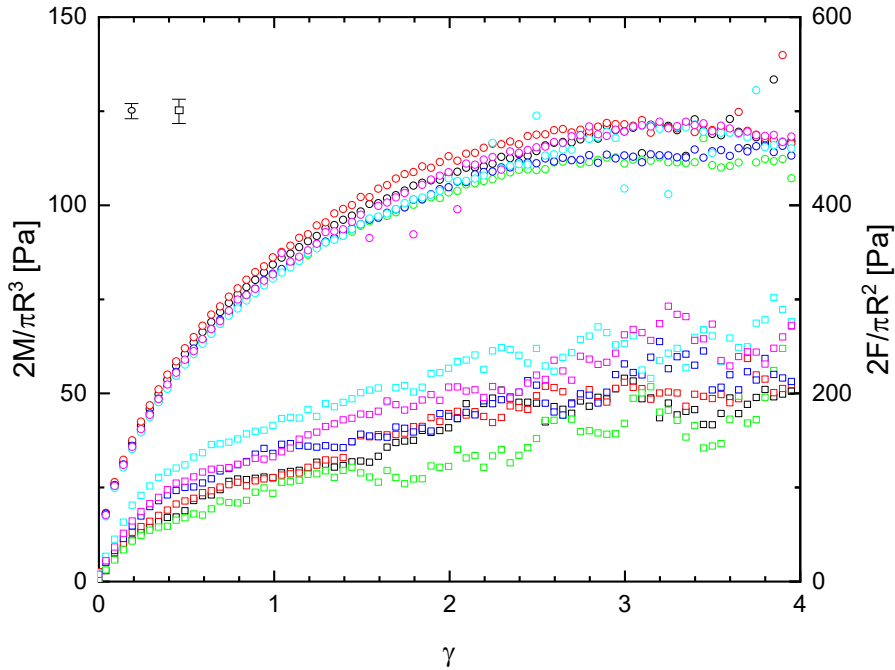
Figure 3.18 Shear stress σ ($\circ$) and $N_1 - N_2$ ($\square$) from constant shear rate ($\dot{\gamma} = 0.01 s^{-1}$) experiments after a recovery period conducted on the MCR301 with parallel-plate geometry. Error bars represent estimated error in computed quantities.
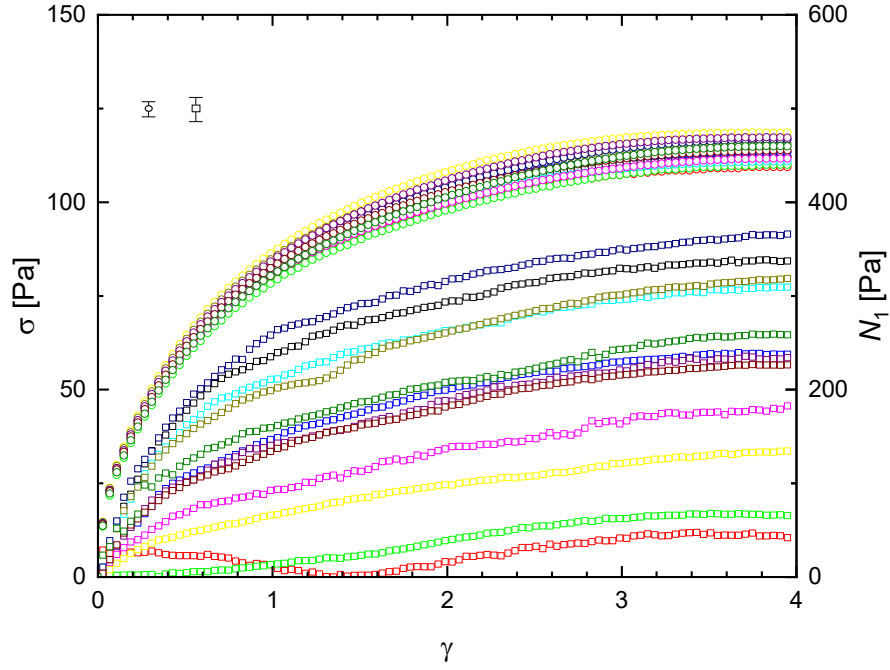
Figure 3.19 Shear stress σ ($\circ$) and $N_1 - N_2$ ($\square$) from constant shear rate ($\dot{\gamma} = 1.0s^{-1}$) experiments after a recovery period conducted on the MCR301 with parallel-plate geometry. Error bars represent estimated error in computed quantities.

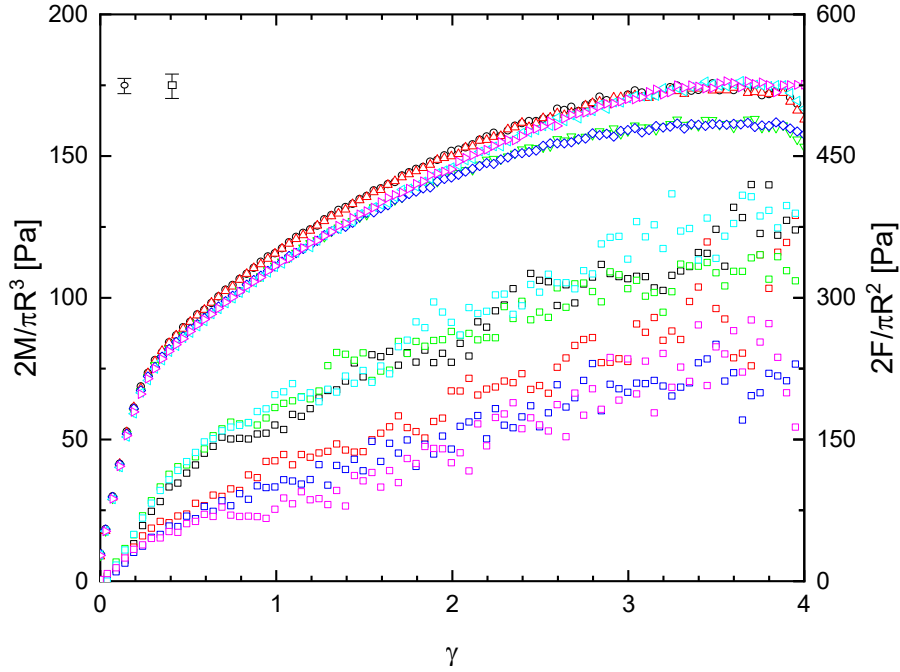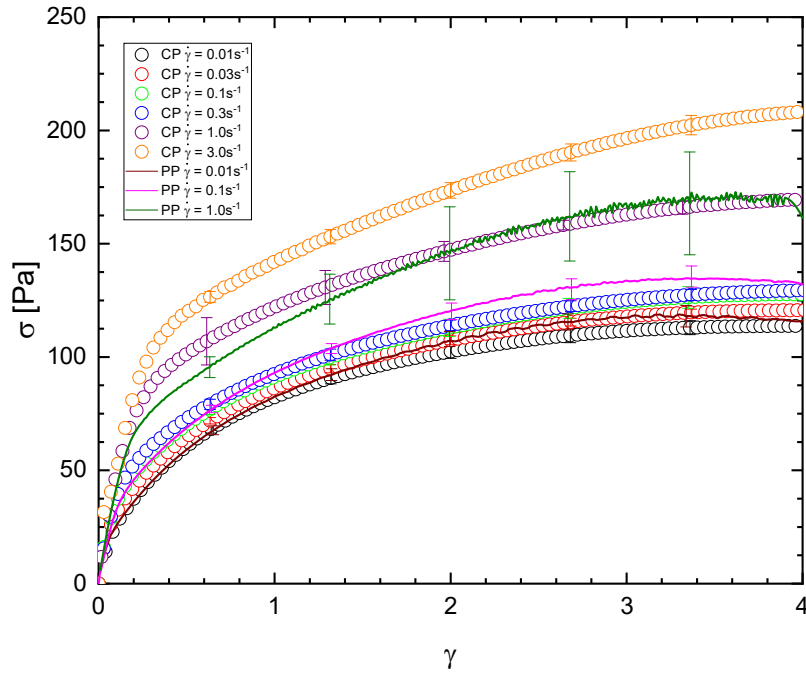**Figure 3.20** Average σ from cone-plate ($\circ$) and calculated parallel-plate recovery experiments at multiple shear rates (curves.) Different colors indicate different shear rates. Error bars represent standard deviations from measurements.

For shear rates below $\dot{\gamma} \leq 0.3s^{-1}$, there is a small increase in stress with shear rate. Cone-plate and parallel plate results agree at these shear rates; however, they remain well below observed relaxation stress values. As the shear rate is increased from $\dot{\gamma} = 1.0s^{-1}$ to $\dot{\gamma} = 3.0s^{-1}$, a large increase in stress values is observed with only the highest shear rate achieving stress values equivalent to that of the relaxation experiments. This increased stress response in relation to increasing shear rate is commonly discussed previous research [45, 50-52, 60, 61]. This behavior is attributed to the reduction in particle cohesion that occurs as the shear rate is increased [60].

Normal stresses do not demonstrate such a clear relationship with shear rate during constant rate experiments. Their growth is also shown in Figures 3.13 - 3.19 for all shear rates, and their averages shown in Figure 3.21. It is apparent that for all shear rates, $N_1 > 0$ was observed, but unlike the shear stress there is not a direct relationship with shear rate. The lowest shear rates tested with the cone plate geometry ($\dot{\gamma} = 0.01s^{-1}$ and $\dot{\gamma} = 0.03s^{-1}$) show similar magnitudes of N_1 as those tested with the highest shear rates ($\dot{\gamma} = 1.0s^{-1}$ and $\dot{\gamma} = 3.0s^{-1}$.) This may have to do with the difference in aging response between flows conducted at low and high shear rates. Negi and Osuji [60] suggests that a colloidal gel subjected to very low shear rates may not be completely fluidized, whereas those subjected to high shear rates achieves a completely fluidized state. They discuss that a fluid subjected to high shear rates displays the full aging response upon flow cessation that rapidly jams the colloidal structure returning it to the glassy state. In contrast, a fluid subjected to low shear rates maintains some of its elastic solid character throughout the duration of flow, therefore resulting in the buildup of internal stresses in the solid-like state, and never fully again upon flow cessation. This could provide an

explanation for the large N_1 values observed at shear rates $\dot{\gamma} = 0.01s^{-1}$ and $\dot{\gamma} = 0.03s^{-1}$. These large values are also seen based on steady state values of the shear and normal stresses shown in Figure 3.22, where N_1 values from cone-plate experiments at low shear rates have similar steady state values to those conducted at the highest shear rates, as previously discussed. This trend does not hold throughout N_1 measurements, and shear stress and $N_1 - N_2$ data collected using the parallel plate geometry, where there appears to be a consistent increase of the stress magnitude as the shear rate is increased.

The strain and normal stress were recorded during recovery periods, and the data is presented in Figures 3.23 and 3.24 (normal stress recovery plots for all shear rates and test geometries shown in Appendix A.) Upon cessation of the flow, both the strain and the normal stresses instantaneously recover some amount, with experiments conducted at higher shear rates demonstrating a greater amount of recovery, in agreement with results in the literature [59, 62, 63]. The recovered strain ranges from ~0.5% ($\dot{\gamma} = 0.01s^{-1}$) to ~20% ($\dot{\gamma} = 3.0s^{-1}$). The normal stresses, however, did not display such a clear relationship between the shear rate and amount of recovery. There is some correlation between the two, with samples subjected to higher shear rates decreasing a slightly greater amount (~280 Pa) than those subjected to lower shear rates (~200Pa.) This could be again related to the above phenomenon described by Negi and Osuji [60], where the lowest shear rate experiments recover less due a greater retention of solid-like characteristics, while the largest shear rates are returning to a solid state after complete fluidization.
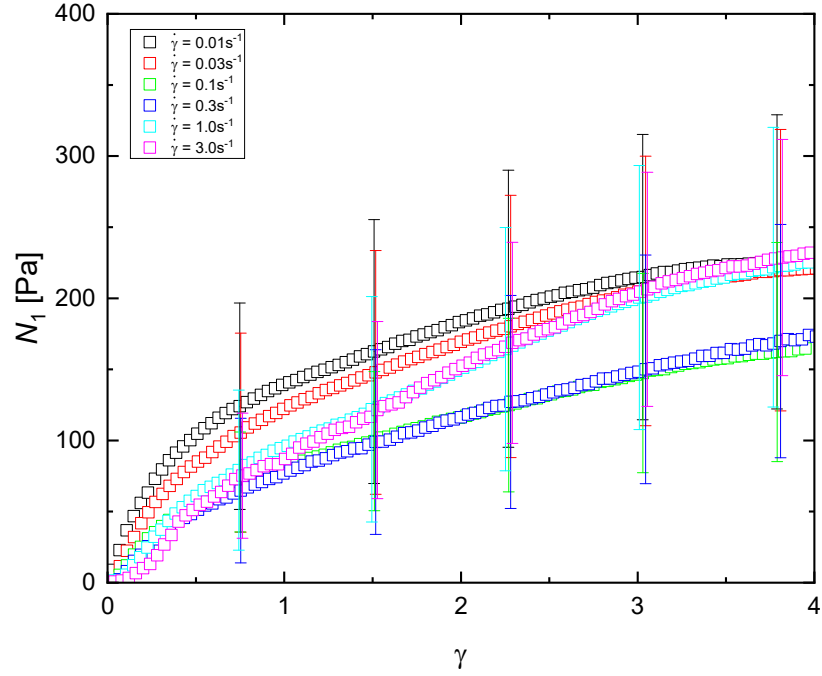
Figure 3.21 N_1 behavior during constant rate experiments following recovery intervals using cone-plate geometry. Error bars represent standard deviations in calculations.

The strain appears to approach a constant value during this time. As stated above most of the strain recovery occurs instantaneously, then continues to recover a small amount until the next constant rate experiment. Upon cessation of the flow, extended polymer chains experience a rapid retraction to their equilibrium contour length followed by a more gradual relaxation of relative chain motion [64]. This phenomenon is well described in the literature for recovery experiments, as the strain approaches a steady state value [7, 59, 62].
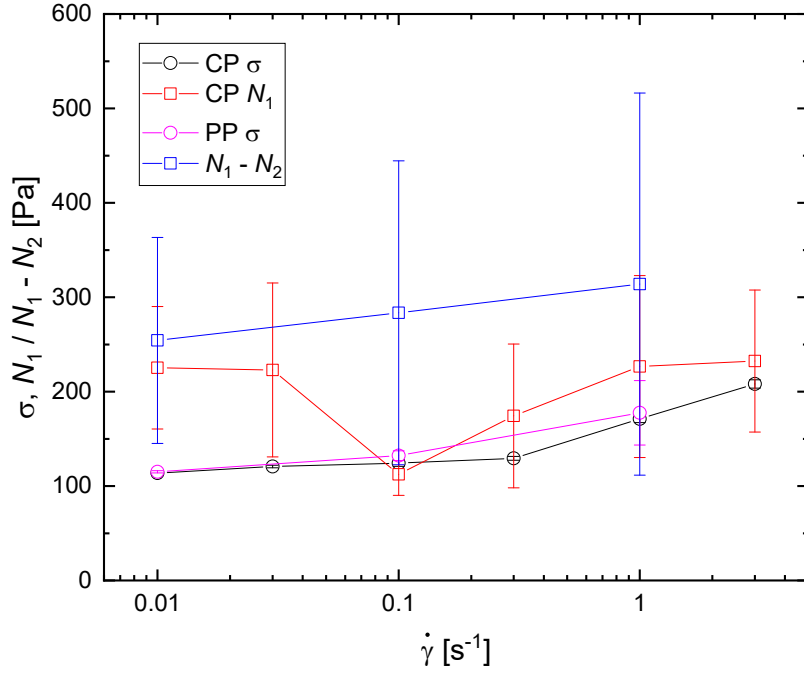
Figure 3.22 Steady state values of σ (cone-plate ○, parallel-plate ○), N_1 (□) and $N_1 - N_2$ (□) for cone plate and parallel plate geometries. Error bars represent standard deviations from calculations.
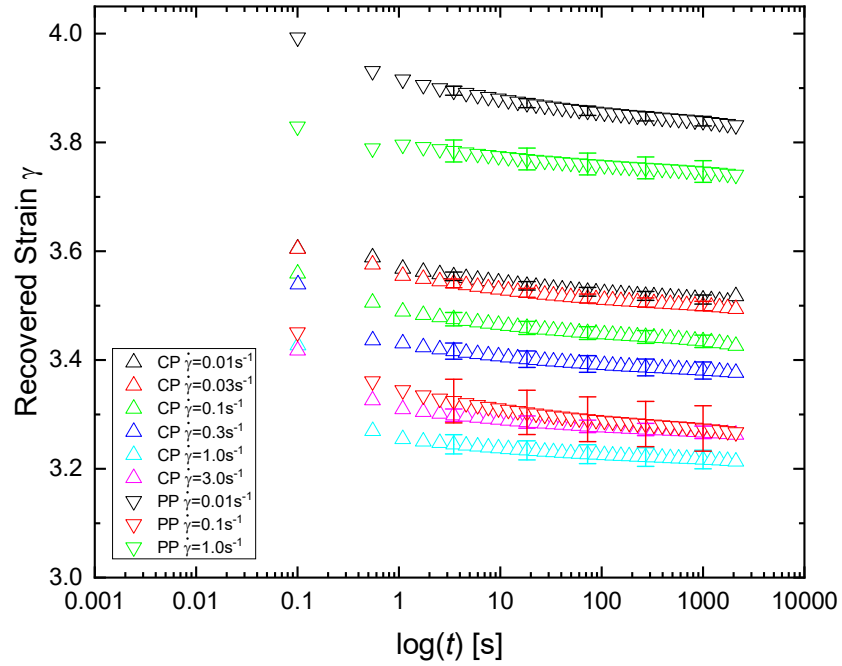
Figure 3.23 Recovered strain profiles during recovery intervals as measured. Error bars represent standard deviations of measurements.

Normal stresses do not approach a steady state value, and little mention of their behavior during recovery experiments is mentioned in the literature. Throughout the recovery period, the normal stresses continue to decrease through the entire period but never reach a steady or zero value. As previously mentioned, others have discussed that normal stresses may never fully relax on moderate timescale, making it difficult to determine the necessary time for complete relaxation.. What is clear, however, is that the material is elastically contracting during these time periods. The growth of normal stresses that occurs during constant shear rate experiments is reversed as the material continues to recover. The conditions under which this contraction occurs seem to have an impact on the behavior of normal stress measurements in subsequent experiments.
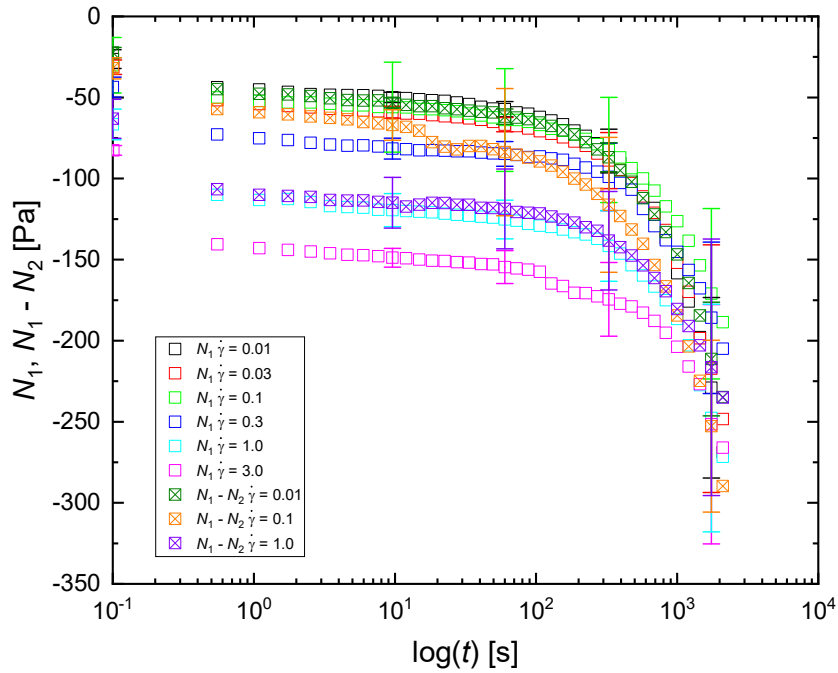
Figure 3.24 Average recovery profiles of N_1 (□) and $N_1 - N_2$ (⊠) for cone-plate and parallel plate experiments. Different colors represent different shear rates. Error bars represent standard deviation of measurements.

To understand how the shear and normal stress develop during constant shear rate experiments, statistics were collected for relaxation and recovery experiments conducted at the shear rate $\dot{\gamma} = 0.1s^{-1}$. To determine the deviation of runs from the average for both the shear and normal stress, the following equations were utilized

$$\Delta\sigma = \frac{\sigma_i - \sigma_{avg}}{\sigma_{avg}} \tag{3.1}$$

$$\Delta N_1 = \frac{N_{1,i} - N_{1,avg}}{N_{1,avg}} \tag{3.2}$$

where $\Delta\sigma$ and ΔN_1 are the deviation of individual shear and normal stress data from the average for constant rate experiments, respectively, σ_{avg} and $N_{1,avg}$ are the average values of the shear and normal stress, and σ_i and $N_{1,i}$ are individual data points from constant rate experiments for the shear and normal stress, respectively. A normal distribution was then fit to the data using the equation

$$f(x) = \frac{1}{s\sqrt{2\pi}} e^{-\frac{1}{2}\left(\frac{x-\mu}{s}\right)^2} \tag{3.3}$$

where s is the standard deviation, x is the data point, and μ is the mean. Standard deviation (SD) and variance (v) values were calculated for the associated datasets using

$$SD = \sqrt{\frac{\Sigma(x_i - \mu)^2}{N}} \tag{3.4}$$

61

$$v = SD^2 \qquad\qquad (3.5)$$

where x_i *is* the individual data point, and N is the size of the dataset. The calculations of the standard deviations and variance values are shown in Table 3.1, and the histograms for the relaxation and recovery experiments from Figure 3.5 and 3.7 are plotted in Figures 3.25 and 3.26, respectively. When comparing the statistics of σ from the two experiments, it is observed that recovery experiments resulted in a slightly larger standard deviation and variance around the average but are on similar orders of magnitude as relaxation results. However, the difference is not statistically significant and both experiments demonstrate good reproducibility of shear stress measurements. Both data sets were fit with normal distribution curves and appear to behave in a Gaussian manner with good symmetry about the mean.

N_1 however demonstrates vastly different behavior between the relaxation and recovery experiments. When comparing standard deviation and variance values presented in Table 3.1, the standard deviation for recovery decreases by a factor of ~5, while the variance is reduced by a factor of ~26. This is a significant change in the behavior of normal stresses and further emphasizes the observed reduction in their chaotic behavior that is seen in Figure 3.7. Again, both histograms were fitted with a normal distribution curve, where the N_1 measurements from relaxation experiments demonstrate greater Gaussian behavior than recovery data. Though the recovery experiments do not clearly demonstrate such clear symmetry about the average as the relaxation data, what is clear and evident is that the recovery conditions had a significant impact on the behavior of N_1 during subsequent shear flow experiments.

The results suggest that residual normal stresses present after a recovery period can influence the yielding behavior of the yield stress fluid. The sample retains a memory of the remaining normal stresses, which become more uniform as the sample is subjected to higher strain levels. These findings provide additional support to the hypothesis that a recovery period may offer favorable conditions for microstructural rearrangement compared to relaxation. Consequently, this promotes more predictable behavior of normal stresses.

Table 3.1 Comparison of Standard Deviation and Variance Values for σ and N_1 from Relaxation and Recovery Experiments Conducted at $\dot{\gamma} = 0.1s^{-1}$

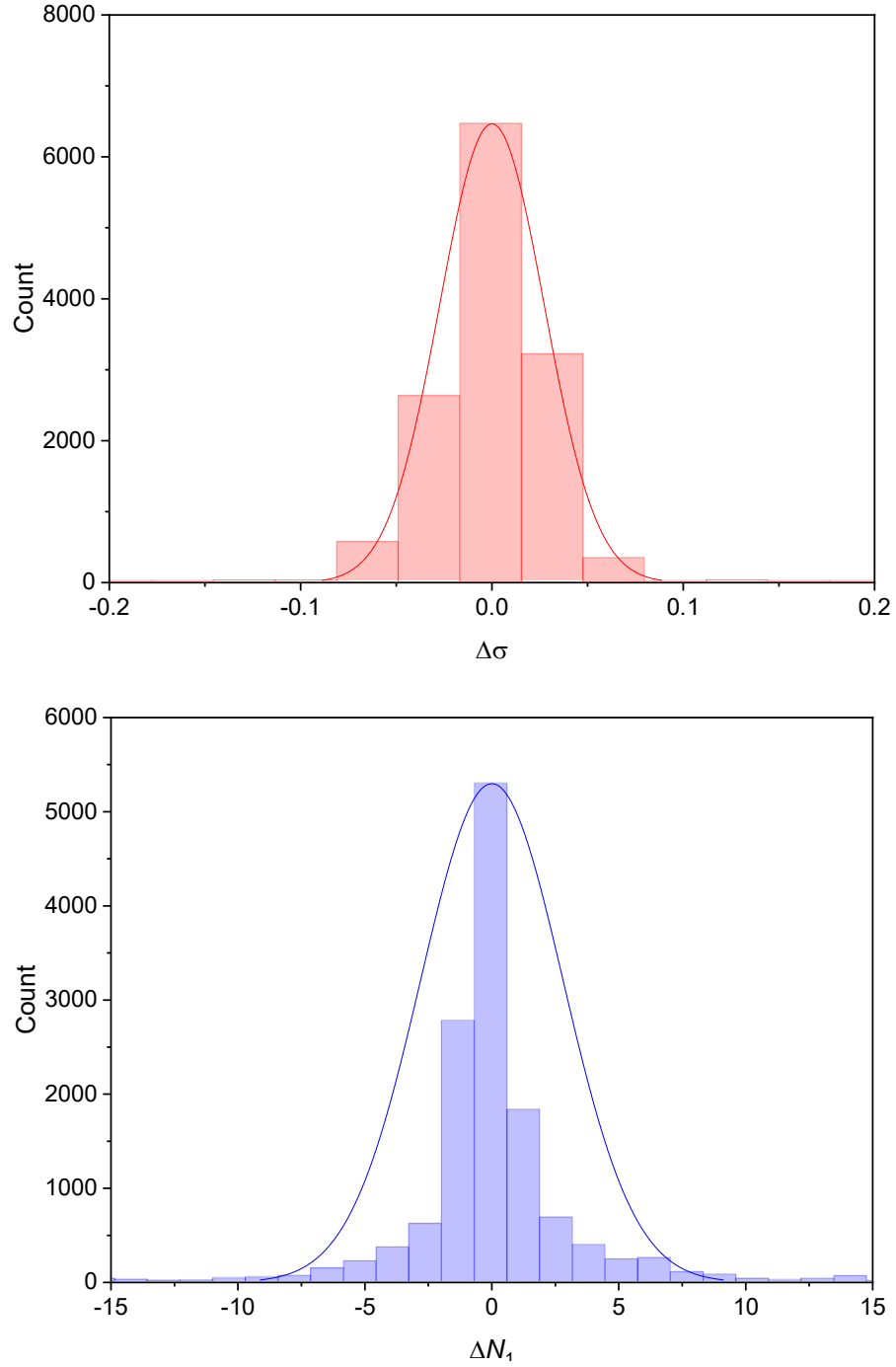|	Standard Deviation σ	Variance σ	Standard Deviation N_1	Variance N_1
Relaxation	0.02729	0.00074	2.80268	7.85503
Recovery	0.03361	0.00113	0.54041	0.29204

Figure 3.25 Average deviation of σ (top) and N_1 (bottom) from cone-plate relaxation experiments ($\dot{\gamma} = 0.1 s^{-1}$) on the RMS800.
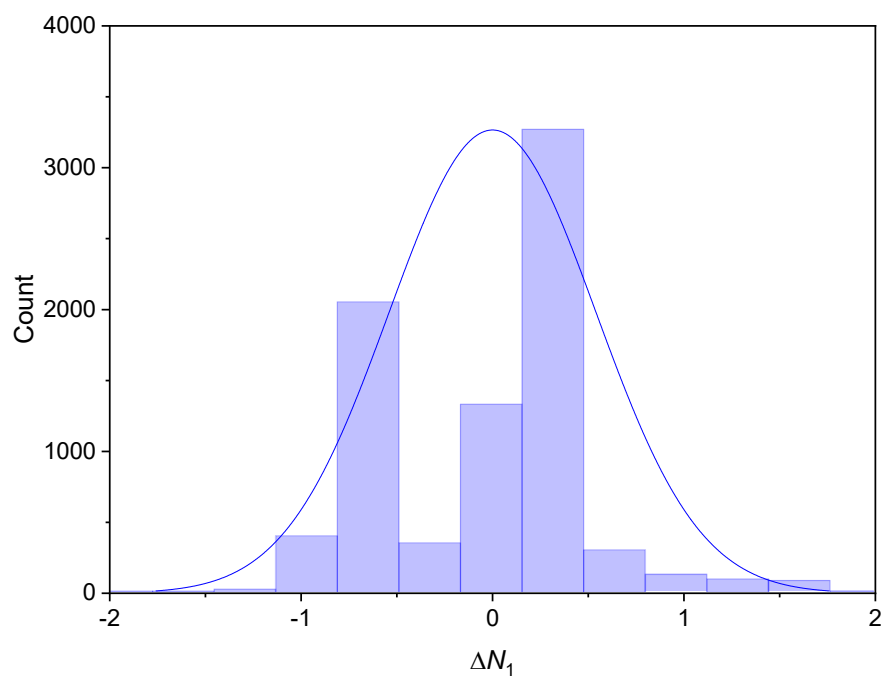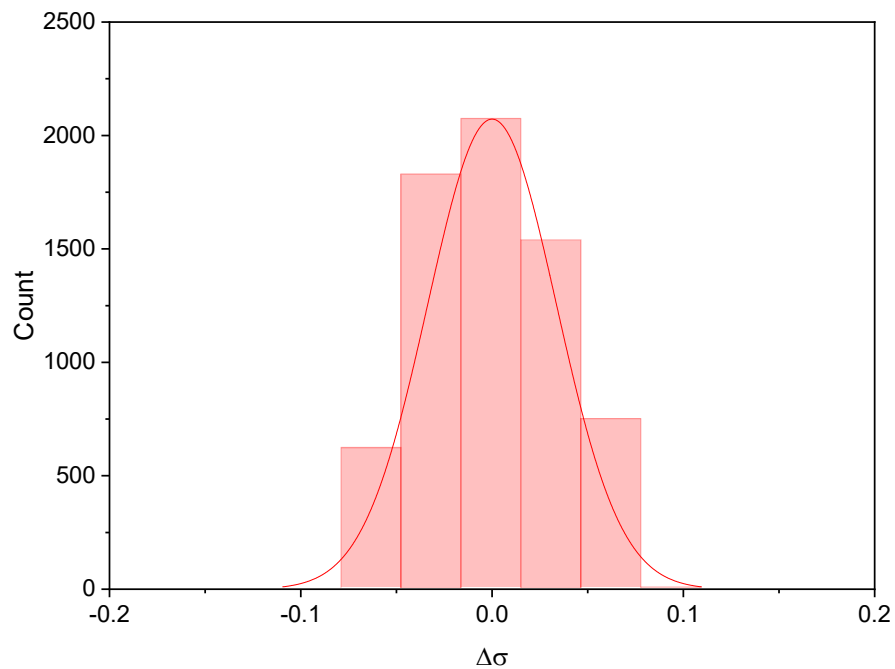
Figure 3.26 Average deviation of σ (top) and N_1 (bottom) from cone-plate recovery experiments ($\dot{\gamma} = 0.1 s^{-1}$) on the MCR301.

CHAPTER 4

CONCLUSION AND FUTURE CONSIDERATIONS

The obtained results clearly demonstrate that the flow behavior of yield stress fluids is influenced not only by flow history but also by the rest period between shear flow experiments. Despite Carbopol being a nonthixotropic yield stress fluid, there is compelling evidence suggesting a relationship between rest periods and the rheological behavior observed in repeat measurements of the system. Shear stress measurements reveal a decrease in the equilibrium stress value attained by the system when subjected to relaxation intervals compared to recovery intervals. Additionally, there is an apparent reduction in the resulting yield stress. The findings from the recovery experiments further support the notion that repeat measurements of normal stress can be more consistent and repeatable compared to measurements obtained solely from relaxation periods. The behavior of normal stress in subsequent experiments is highly dependent on the rest conditions applied between tests, allowing the system to relax towards its original state as much as possible. The study highlights the importance of carefully considering the conditions required for appropriate structural rearrangements, enabling the fluid to return to a state that closely resembles its initial configuration before subsequent flow experiments are conducted within a reasonable timeframe.

To gain a deeper understanding of the observed changes in shear and normal stress behavior, further testing is necessary. It is crucial to explore various combinations of flow experiments and rest periods to unravel the factors contributing to the apparent changes in flow behavior. This should extend to a wider range of complex fluids, such as emulsions, foams, and suspensions, which exhibit diverse flow behaviors due to various

microstructural arrangements. By conducting additional testing while considering these factors, it is possible to advance our understanding of the rheological behavior of complex fluids. This will provide valuable insights into the intricate dynamics of these materials, allowing for improved models and theories that accurately describe their flow behavior.

APPENDIX A

ADDITIONAL FIGURES

This appendix contains plots of normal stress measurements made during recovery intervals at each of the various shear rates mentioned above. The average of each of the following plots is presented in Figure 3.21.

Figure A.1 Recovery profiles of N_1 ($\square$) for cone-plate experiments at $\gamma = 0.01s^{-1}$. Error bar represents error propagation from computed quantities.

Figure A.2 Recovery profiles of N_1 (□) for cone-plate experiments at $\gamma = 0.03s^{-1}$. Error bar represents error propagation from computed quantities.

Figure A.3 Recovery profiles of N_1 (□) for cone-plate experiments at $\gamma = 0.1s^{-1}$ Error bar represents error propagation from computed quantities.
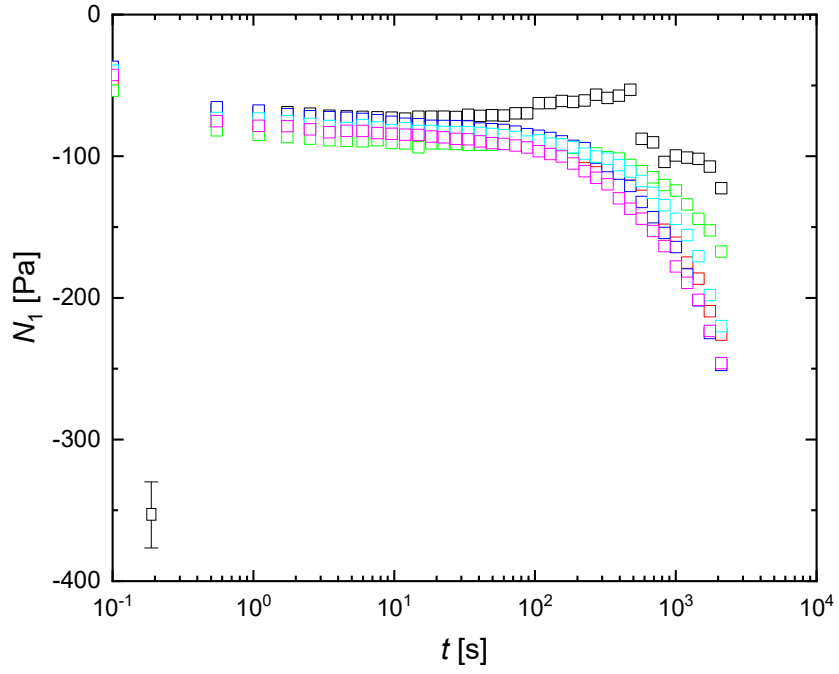
Figure A.4 Recovery profiles of N_1 ($\square$) for cone-plate experiments at $\gamma = 0.3s^{-1}$ Error bar represents error propagation from computed quantities.
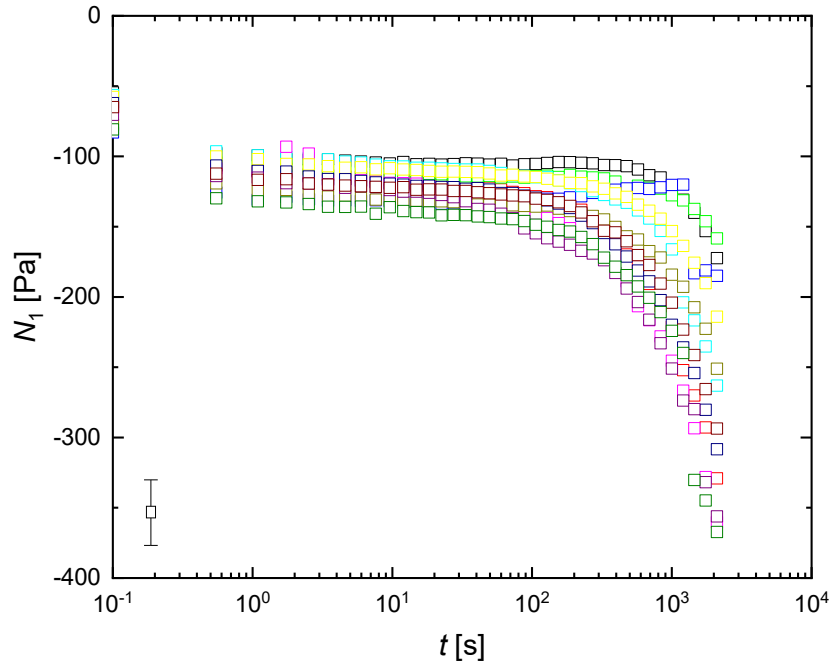
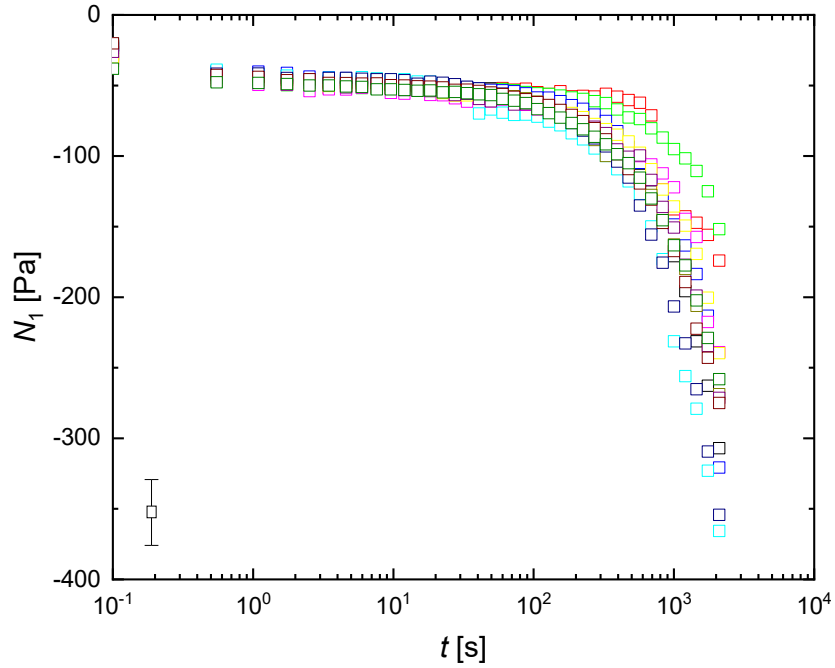

Figure A.5 Recovery profiles of N_1 ($\square$) for cone-plate experiments at $\gamma = 1.0s^{-1}$. Error bar represents error propagation from computed quantities.
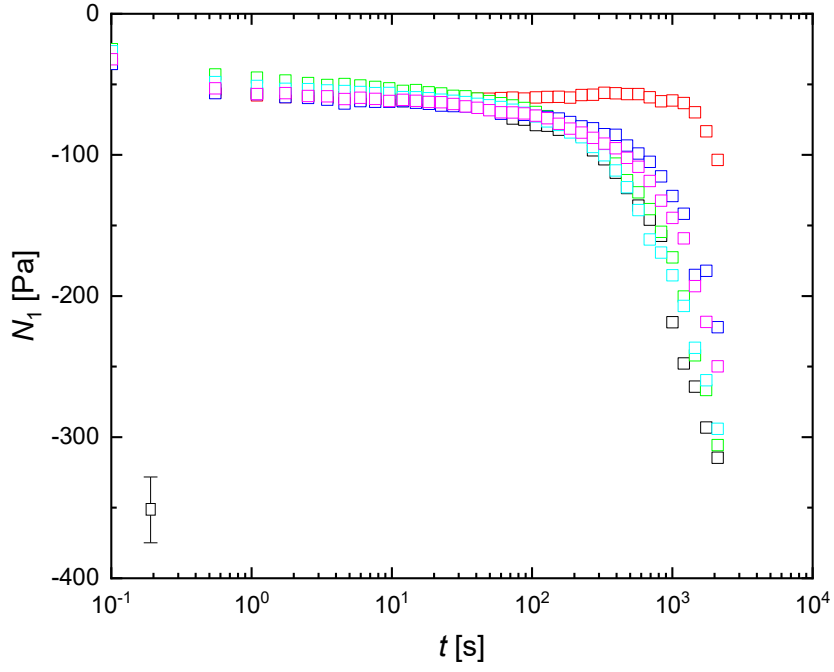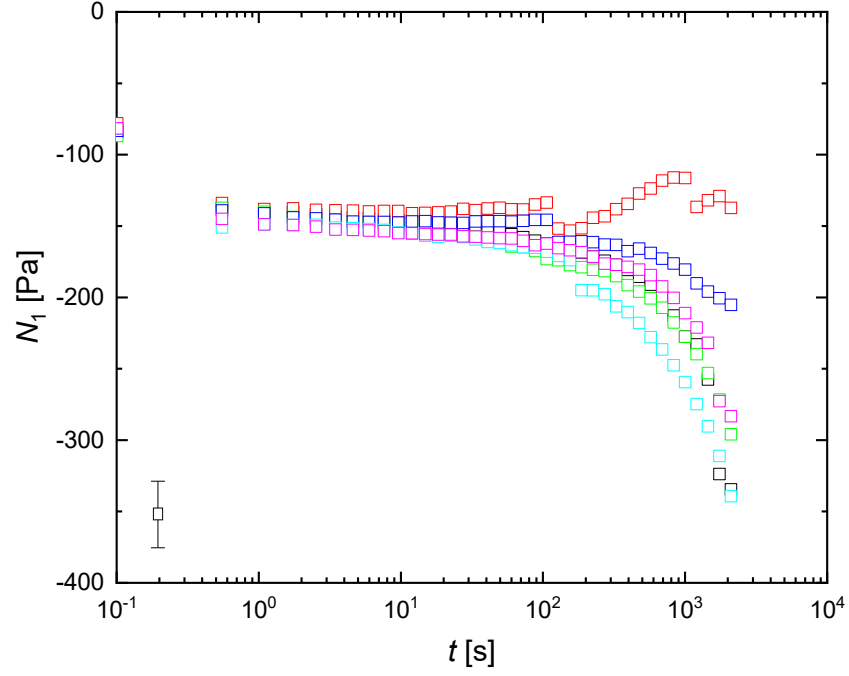
Figure A.6 Recovery profiles of N_1 ($\square$) for cone-plate experiments at $\gamma = 3.0 s^{-1}$ Error bar represents error propagation from computed quantities.
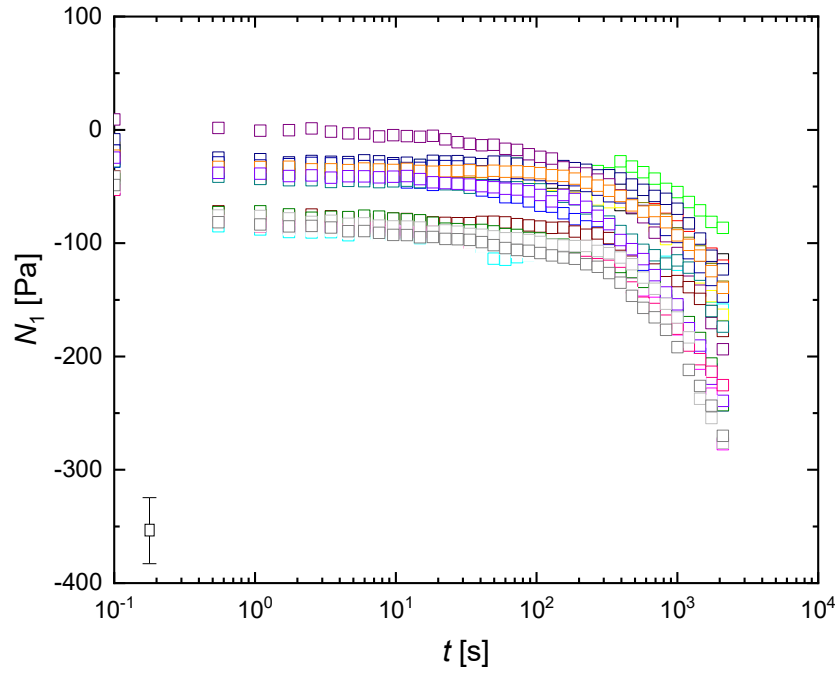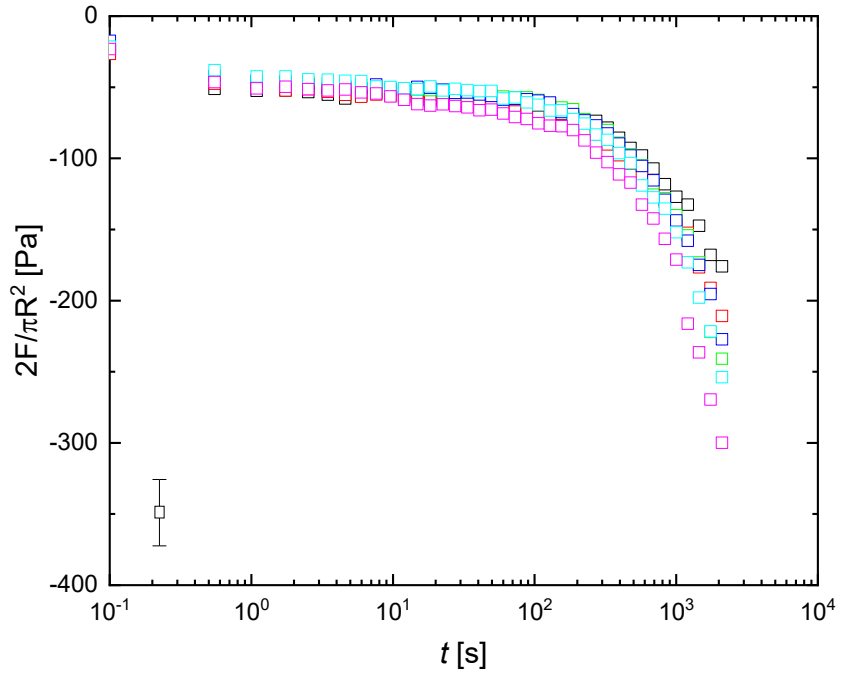

Figure A.7 Recovery profiles of $N_1 - N_2$ ($\square$) for parallel-plate experiments at $\gamma = 0.01 s^{-1}$. Error bar represents error propagation from computed quantities.

Figure A.8 Recovery profiles of $N_1 - N_2$ ($\square$) for parallel-plate experiments at $\gamma = 0.1 s^{-1}$. Error bar represents error propagation from computed quantities.

Figure A.9 Recovery profiles of $N_1 - N_2$ ($\square$) for parallel-plate experiments at $\gamma = 1.0 s^{-1}$. Error bar represents error propagation from computed quantities.
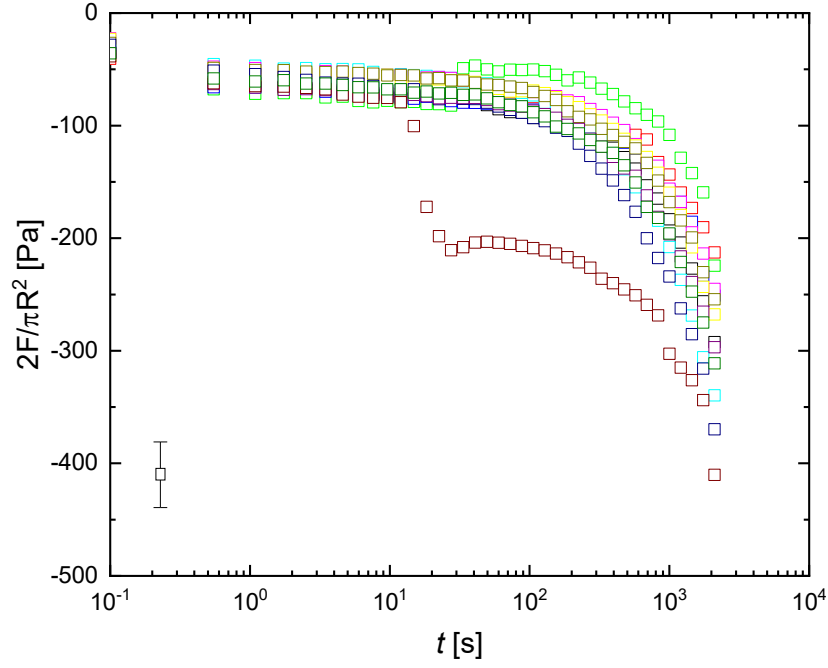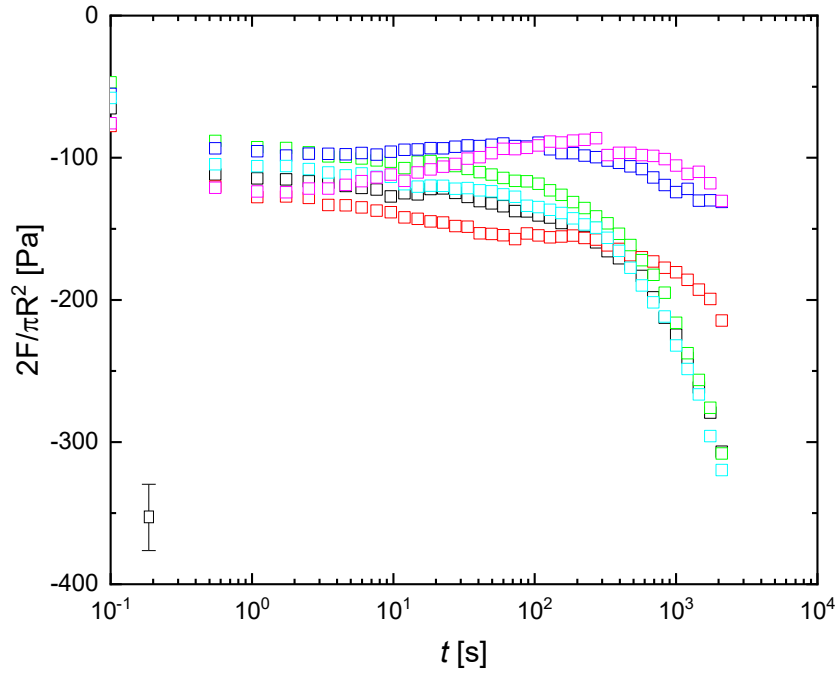
REFERENCES

[1] H. Ramli, N.F.A. Zainal, M. Hess, C.H. Chan, Basic principle and good practices of rheology for polymers for teachers and beginners, Chemistry Teacher International 4(4) (2022) 307-326.

[2] D. Bonn, M.M. Denn, L. Berthier, T. Divoux, S. Manneville, Yield stress materials in soft condensed matter, Reviews of Modern Physics 89(3) (2017) 035005.

[3] P. Møller, A. Fall, V. Chikkadi, D. Derks, D. Bonn, An attempt to categorize yield stress fluid behaviour, Philosophical transactions. Series A, Mathematical, physical, and engineering sciences 367 (2009) 5139-55.

[4] E. Di Giuseppe, F. Corbi, F. Funiciello, A. Massmeyer, T.N. Santimano, M. Rosenau, A. Davaille, Characterization of Carbopol® hydrogel rheology for experimental tectonics and geodynamics, Tectonophysics 642 (2015) 29-45.

[5] M. Instruments, A basic introduction to rheology, Malvern Instruments Limited: Worcestershire, UK (2016).

[6] D.C. Venerus, H.C. Öttinger, A modern course in transport phenomena, Cambridge University Press2018.

[7] M. Rubinstein, R.H. Colby, Polymer physics, Oxford university press New York2003.

[8] F.A. Morrison, Understanding rheology, Oxford University Press, USA2001.

[9] P. Coussot, Yield stress fluid flows: A review of experimental data, Journal of Non-Newtonian Fluid Mechanics 211 (2014) 31-49.

[10] J.-C. Baret, D. Vandembroucq, S. Roux, Extremal Model for Amorphous Media Plasticity, Physical Review Letters 89(19) (2002) 195506.

[11] G. Picard, A. Ajdari, L. Bocquet, F. Lequeux, Simple model for heterogeneous flows of yield stress fluids, Physical Review E 66(5) (2002) 051501.

[12] G. Picard, A. Ajdari, F. Lequeux, L. Bocquet, Slow flows of yield stress fluids: Complex spatiotemporal behavior within a simple elastoplastic model, Physical Review E 71(1) (2005) 010501.

[13] L. Bocquet, A. Colin, A. Ajdari, Kinetic Theory of Plastic Flow in Soft Glassy Materials, Physical Review Letters 103(3) (2009) 036001.

[14] V. Labiausse, R. Hohler, S. Cohen-Addad, Shear induced normal stress differences in aqueous foams, Journal of Rheology 51 (2006).

[15] F. Ahonguio, L. Jossic, A. Magnin, Influence of surface properties on the flow of a yield stress fluid around spheres, Journal of Non-Newtonian Fluid Mechanics 206 (2014) 57-70.

[16] A. Fall, B.P. Tighe, D. Bonn, Tuneable normal stresses in hyperelastic emulsions, Physical Review Research 4(1) (2022) 013167.

[17] L. Bécu, S. Manneville, A. Colin, Yielding and Flow in Adhesive and Nonadhesive Concentrated Emulsions, Physical Review Letters 96(13) (2006) 138302.

[18] B. Dollet, C. Raufaste, Rheology of aqueous foams, Comptes Rendus Physique 15(8) (2014) 731-747.

[19] K. Masschaele, J. Fransaer, J. Vermant, Flow-induced structure in colloidal gels: direct visualization of model 2D suspensions, Soft Matter 7(17) (2011) 7717-7726.

[20] S. Hutzler, W. Drenckhan, A. Saugey, S. Cox, The Rheology of Foams, (2006).

[21] G. Ovarlez, L. Tocquer, F. Bertrand, P. Coussot, Rheopexy and tunable yield stress of carbon black suspensions, Soft Matter 9(23) (2013) 5540-5549.

[22] H.A. Barnes, Q.D. Nguyen, Rotating vane rheometry — a review, Journal of Non-Newtonian Fluid Mechanics 98(1) (2001) 1-14.

[23] D.C. Venerus, O. Machabeli, D. Bushiri, S.M. Arzideh, Evidence for Chaotic Behavior during the Yielding of a Soft Particle Glass, Physical Review Letters 129(6) (2022) 068002.

[24] M. Keentok, The measurement of the yield stress of liquids, Rheologica Acta 21(3) (1982) 325-332.

[25] K. Hyun, M. Wilhelm, C.O. Klein, K.S. Cho, J.G. Nam, K.H. Ahn, S.J. Lee, R.H. Ewoldt, G.H. McKinley, A review of nonlinear oscillatory shear tests: Analysis and application of large amplitude oscillatory shear (LAOS), Progress in Polymer Science 36(12) (2011) 1697-1753.

[26] K. Hyun, J.G. Nam, M. Wilhelm, K.H. Ahn, S.J. Lee, Nonlinear response of complex fluids under LAOS (large amplitude oscillatory shear) flow, Korea-australia Rheology Journal 15 (2003) 97-105.

[27] M. Wilhelm, Fourier-Transform Rheology, Macromolecular Materials and Engineering 287(2) (2002) 83-105.

[28] E.C. Bingham, An investigation of the laws of plastic flow, US Government Printing Office1917.

[29] W.H. Herschel, R. Bulkley, Konsistenzmessungen von Gummi-Benzollösungen, Kolloid-Zeitschrift 39(4) (1926) 291-300.

[30] M. Instruments, Understanding yield stress measurements, 2012.

[31] J.G. Oldroyd, A rational formulation of the equations of plastic flow for a Bingham solid, Mathematical Proceedings of the Cambridge Philosophical Society, Cambridge University Press, 1947, pp. 100-105.

[32] R.B. Bird, R.C. Armstrong, O. Hassager, Dynamics of polymeric liquids. Vol. 1: Fluid mechanics, (1987).

[33] C. Macosko, Rheology principles, measurements, and applications, VCH Publ, Inc, New York (1994).

[34] J.-Y. Kim, J.-Y. Song, E.-J. Lee, S.-K. Park, Rheological properties and microstructures of Carbopol gel network system, Colloid and Polymer Science 281(7) (2003) 614-623.

[35] J.M. Piau, Carbopol gels: Elastoviscoplastic and slippery glasses made of individual swollen sponges: Meso- and macroscopic properties, constitutive equations and scaling laws, Journal of Non-Newtonian Fluid Mechanics 144(1) (2007) 1-29.

[36] Z. Jaworski, T. Spychaj, A. Story, G. Story, Carbomer microgels as model yield-stress fluids, Reviews in Chemical Engineering 38(7) (2022) 881-919.

[37] J.O. Carnali, M.S. Naser, The use of dilute solution viscometry to characterize the network properties of carbopol microgels, Colloid and Polymer Science 270(2) (1992) 183-193.

[38] A. Gómez-Carracedo, C. Alvarez-Lorenzo, J.L. Gómez-Amoza, A. Concheiro, Glass transitions and viscoelastic properties of carbopol and noveon compacts, Int J Pharm 274(1-2) (2004) 233-43.

[39] N.W. Taylor, E.B. Bagley, Dispersions or solutions? A mechanism for certain thickening agents, Journal of Applied Polymer Science 18(9) (1974) 2747-2761.

[40] T.L. Corporation, Moleuclar Weight of Carbopol and Pemulen Polymers, Technical Report TDS-222, 2007.

[41] F.I. Safitri, D. Nawangsari, D. Febrina, Overview: Application of Carbopol 940 in Gel, Atlantis Press, 2021, pp. 80-84.

[42] C.F. Chemical, Carbopol 940 Product Specification. https://www.cdhfinechemical.com/images/product/specs/37_328378222_CARBOPOL940_CAS NO-9003-01-4_044275.pdf. (Accessed May 17 2023).

[43] P. R. Varges, C. M. Costa, B. S. Fonseca, M. F. Naccache, P.R. De Souza Mendes, Rheological Characterization of Carbopol® Dispersions in Water and in Water/Glycerol Solutions, Fluids 4(1) (2019) 3.

[44] M.T. Islam, N. Rodríguez-Hornedo, S. Ciotti, C. Ackermann, Rheological characterization of topical carbomer gels neutralized to different pH, Pharm Res 21(7) (2004) 1192-9.

[45] B.W. Barry, M.C. Meyer, The rheological properties of carbopol gels I. Continuous shear and creep properties of carbopol gels, International Journal of Pharmaceutics 2(1) (1979) 1-25.

[46] B.W. Barry, M.C. Meyer, The rheological properties of carbopol gels II. Oscillatory properties of carbopol gels, International Journal of Pharmaceutics 2(1) (1979) 27-40.

[47] P. Coussot, Rheophysics of pastes: a review of microscopic modelling approaches, Soft Matter 3(5) (2007) 528-540.

[48] H.d. Cagny, M. Fazilati, M. Habibi, M.M. Denn, D. Bonn, The yield normal stress, Journal of Rheology 63(2) (2019) 285-290.

[49] M. Habibi, M. Dinkgreve, J. Paredes, M.M. Denn, D. Bonn, Normal stress measurement in foams and emulsions in the presence of slip, Journal of Non-Newtonian Fluid Mechanics 238 (2016) 33-43.

[50] F. Cocchini, M.R. Nobile, D. Acierno, Transient and steady rheological behavior of the thermotropic liquid crystal copolymer 73/27 HBA/HNA, Journal of Rheology 35(6) (1991) 1171-1189.

[51] H.C. Langelaan, A.D. Gotsis, The relaxation of shear and normal stresses of nematic liquid crystalline polymers in squeezing and shear flows, Journal of Rheology 40(1) (1996) 107-129.

[52] P. Lidon, L. Villa, S. Manneville, Power-law creep and residual stresses in a carbopol gel, Rheologica Acta 56(3) (2017) 307-323.

[53] R.L. Thompson, L.U.R. Sica, P.R. de Souza Mendes, The yield stress tensor, Journal of Non-Newtonian Fluid Mechanics 261 (2018) 211-219.

[54] C.M. Vrentas, W.W. Graessley, Relaxation of shear and normal stress components in step-strain experiments, Journal of Non-Newtonian Fluid Mechanics 9(3) (1981) 339-355.

[55] T. Schweizer, A. Bardow, The role of instrument compliance in normal force measurements of polymer melts, Rheologica Acta 45(4) (2006) 393-402.

[56] D.C. Venerus, R. Nair, Stress relaxation dynamics of an entangled polystyrene solution following step strain flow, Journal of Rheology 50(1) (2006) 59-75.

[57] D.C. Venerus, A critical evaluation of step strain flows of entangled linear polymer liquids, Journal of Rheology 49(1) (2005) 277-295.

[58] P. Møller, A. Fall, D. Bonn, Origin of apparent viscosity in yield stress fluids below yielding, Europhysics Letters 87(3) (2009) 38004.

[59] J.M. Dealy, D.J. Read, R.G. Larson, Structure and rheology of molten polymers: from structure to flow behavior and back again, Carl Hanser Verlag GmbH Co KG2018.

[60] A.S. Negi, C.O. Osuji, Physical aging and relaxation of residual stresses in a colloidal glass following flow cessation, Journal of Rheology 54 (2010) 943-958.

[61] M. Dinkgreve, M.M. Denn, D. Bonn, "Everything flows?": elastic effects on startup flows of yield-stress fluids, Rheologica Acta 56(3) (2017) 189-194.

[62] R.J. Ketz, R.K. Prud'homme, W.W. Graessley, Rheology of concentrated microgel solutions, Rheologica Acta 27(5) (1988) 531-539.

[63] S.-Q. Wang, Y. Wang, S. Cheng, X. Li, X. Zhu, H. Sun, New Experiments for Improved Theoretical Description of Nonlinear Rheology of Entangled Polymers, Macromolecules 46(8) (2013) 3147-3159.

[64] D.C. Venerus, H. Kahvand, Normal stress relaxation in reversing double-step strain flowsa), Journal of Rheology 38(5) (1994) 1297-1315.